universität wien

MASTERARBEIT / MASTER'S THESIS

Titel der Masterarbeit / Title of the Master's Thesis

„Assessment of a fully automated system for spectrophotometric and potentiometric pK_a determination"

verfasst von / submitted by

Sarah Luise Stellnberger, BSc

angestrebter akademischer Grad / in partial fulfilment of the requirements for the degree of

Magistra pharmaciae (Mag.pharm.)

Wien, 2023 / Vienna, 2023

Studienkennzahl lt. Studienblatt / degree programme code as it appears on the student record sheet:	UA 066 605
Studienrichtung lt. Studienblatt / degree programme as it appears on the student record sheet:	Masterstudium Pharmazie
Betreut von / Supervisor:	Ass.-Prof. Mag. Dr. Verena Pichler

To my family and friends

Acknowledgement

I would like to take this opportunity to express my deep appreciation to those who have supported me throughout my academic journey and played an important role in making my master's thesis a reality.

First and foremost, I would like to express my sincere gratitude to my supervisor, Ass.-Prof. Mag. Dr. Verena Pichler. Her constant support, guidance, and invaluable feedback were vital in helping me complete this thesis. I have been fortunate to work with such a dedicated and knowledgeable mentor, and I will always be grateful for the opportunity to learn from her.

Secondly, I would like to thank my family for their unwavering love and support throughout my studies. Their encouragement and financial support have been critical in enabling me to pursue my academic goals. I am deeply grateful for their sacrifices, and I know that I would not be where I am today without them.

In addition, I would like to thank the department of pharmaceutical sciences for creating a supportive and intellectually stimulating environment that has promoted my academic growth.

Lastly, I would like to thank my friends for their constant support, motivation, and encouragement. Their positive influence and support have helped me overcome many obstacles and stay focused on my goals.

I am humbled by the support of my supervisor, family, friends, colleagues, and research participants. I am grateful for the opportunity to complete this master's thesis, and I will always cherish the experiences and relationships that have shaped my academic journey.

Zusammenfassung

Diese Masterarbeit bewertet ein vollständig automatisiertes System zur Bestimmung der Säurekonstante (pK_s), welche ein entscheidender physikalisch-chemischer Parameter bei der Arzneimittelforschung und -entwicklung ist. Eine genaue und zuverlässige Messung des pK_s ist unerlässlich, da selbst geringe Abweichungen dieses Parameters einen signifikanten Einfluss auf die Wirksamkeit und Sicherheit eines Arzneimittels haben können.

Die Studie umfasste die Messung der pK_s-Werte von 46 Verbindungen, einschließlich solcher, die die Blut-Hirn-Schranke (BHS) durchdringen, die die BHS nicht durchdringen und Verbindungen, die mit verschiedenen Efflux-Transportern interagieren. Die pK_s-Werte wurden mit sowohl spektrophotometrischen, als auch potentiometrischen Methoden bestimmt, und die gemessenen pK_s-Werte wurden den berechneten Werten gegenüber gestellt, um deren Vergleichbarkeit zu analysieren. Die Ziele des Projekts waren die Bewertung der Genauigkeit und Zuverlässigkeit des vollständig automatisierten SiriusT3-Systems für die spektrophotometrische und potentiometrische pK_s-Bestimmung sowie die Etablierung einer Standardarbeitsanweisung (SOP) für das Instrument und die Software. Das übergeordnete Ziel ist die Bewertung des pK_s für neuentwickelte Substanzen, die im zentralen Nervensystem (ZNS) aktiv sind.

Die Ergebnisse dieser Studie zeigen, dass das SiriusT3-System ein zuverlässiges und genaues Instrument für die Bestimmung von pK_s-Werten ist. Das System ermöglicht eine schnelle Messung der Säurekonstante in nur 6 Minuten mit minimalen Probenmengen und -vorbereitungen, und die erhaltenen Messungen sind hoch reproduzierbar. Die Genauigkeit der gemessenen pK_s-Werte wurde durch den Vergleich der unterschiedlichen Messmethoden, sowie durch den Vergleich mit publizierten Werten bestätigt. Die Ergebnisse betonen die Bedeutung der experimentellen Bestimmung der Säurekonstante und die Wichtigkeit der Verwendung eines zuverlässigen und genauen Instruments wie dem SiriusT3 in diesem Prozess.

Im Zuge dieser Masterarbeit wurde eine Standardarbeitsanweisung entwickelt, welche eine umfassende Anleitung zur Bestimmung der Säurekonstante unter Verwendung des SiriusT3-Instruments und der Software darstellt. Diese Anleitung umfasst detaillierte Anweisungen zur Probenpräparation, zur Instrumentenkalibrierung, zur Datenerfassung und -analyse sowie zur Qualitätskontrolle. Der SOP wird ein nützliches Werkzeug für zukünftige Forscher sein, die mit dem SiriusT3-Instrument arbeiten, um sicherzustellen, dass die Messungen genau, zuverlässig und reproduzierbar sind.

Diese Studie untersuchte auch die Relevanz der Säurekonstante bei der Vorhersage einer potentiellen Aktivität im ZNS. Die Ergebnisse dieser Analyse legen nahe, dass der ZNS-Multiparameter-Optimierungs-Score (CNS MPO-Score) zwar eine erste Einschätzung einer möglichen ZNS-Aktivität zulässt, diese sich aber nur auf passive Diffusion anwenden lässt. Die Ergebnisse verdeutlichen dennoch, dass die Berücksichtigung mehrerer Moleküleigenschaften der isolierten Betrachtung einzelner Parameter überlegen ist.

Die Literatursuche nach veröffentlichten experimentellen Daten zu pK_s-Werten der 46 gemessenen Verbindungen war für viele der Substanzen erfolglos, da nur für wenige Verbindungen experimentelle Daten verfügbar waren. Obwohl diverse physikochemische Parameter auf Webseiten wie PubChem dargestellt werden, sind dennoch kaum pK_s Werte auf diesen Plattformen verfügbar. Die in dieser Studie generierten Messwerte stellen eine Datenbank von experimentell erhobenen pK_s-Werten dar. Die erzielten Daten, sowie die daraus erworbenen Erkenntnisse werden für eine Publikation von Interesse sein, um die Arbeit von Wissenschaftlern und Forschern auf diesem Gebiet zu unterstützen.

Abstract

This master thesis evaluates a fully automated system for the determination of the ionisation constant or pK_a, which is a crucial physicochemical parameter in drug discovery and development. Accurate and reliable measurement of the pK_a is essential, as even small variations in this parameter can have a significant impact on the efficacy and safety of a drug.

This study involved the pK_a-determination of 46 compounds, including blood-brain-barrier (BBB) penetrating and BBB non-penetrating compounds, and substances that interact with various efflux transporters. The pK_a values were determined using both spectrophotometric and potentiometric methods, and the calculated pK_a values were compared with the measured values to assess their validity. The objectives of the project were to assess the accuracy and reliability of the fully automated SiriusT3 system for spectrophotometric and potentiometric pK_a determination, and to establish a standard operating procedure (SOP) for the instrument and software. The overall goal is to evaluate the ionization constant for newly developed compounds that are active in the central nervous system (CNS).

The results of this study demonstrate that the SiriusT3 instrument is a reliable and accurate tool for the determination of the ionisation constant. The system allows for rapid measurement of pK_a values in just 6 minutes with minimal sample quantities and preparation, and the measurements obtained are highly reproducible. The accuracy of the measured pK_a values was confirmed by the comparison of the different measurement methods and comparison to published experimental data. The findings highlight the importance of experimental determination of the pK_a, and the value of using a reliable and accurate instrument such as the SiriusT3 in this process.

The SOP developed within this master thesis provides a comprehensive manual for the determination of the ionisation constant using the SiriusT3 instrument and software. This manual includes detailed instructions for sample preparation, instrument calibration, data acquisition and analysis, and quality control. It will be a useful tool for future researchers working with the SiriusT3, ensuring that the measurements obtained are accurate, reliable, and reproducible.

This work also investigated the relevance of the pK_a in predicting the CNS activity of 46 compounds. The results of this analysis suggest that the CNS multiparameter optimisation score (CNS MPO score), which includes pK_a as one of its six parameters, is a reasonable approach for a first prediction of CNS activity. However, this prediction is only applicable to passive diffusion and does not consider any transport mechanisms. Nevertheless, these findings demonstrate the importance of considering multiple physicochemical parameters, including the pK_a, in predicting the efficacy and safety of a drug.

Furthermore, the literature search for published experimental data on the pK_a values was largely unsuccessful, with data available for only a few of the 46 compounds. Despite the inclusion of various physicochemical parameters on sites such as PubChem, pK_a values are often not displayed on these platforms. Therefore, the data generated in this study and the resulting insights will be of interest for publication, providing a library of experimental pK_a values for well-known therapeutic drugs and supporting the work of scientists and researchers in the field.

Contents

1 Introduction

1.1 Drug discovery and development

The driving motivation behind a drug discovery program is the unmet clinical need for a medical solution to a disease or condition. The initial research focuses on generating data to support the hypothesis that targeting a specific protein or pathway will have a therapeutic effect.

Although many substances are investigated annually, only a small percentage show promise of clinical applicability and are tested on patients. Even fewer reach the market due to the stringent requirements for clinical trials and therapeutic application. (1,2)

The drug discovery process is both time-consuming and expensive, taking over a decade on average and costing more than $2 billion before it becomes available to the public (See figure 1).(3) This is particularly true for neurological drugs, which can take up to 18 years to complete the journey from laboratory evaluation to regulatory approval.

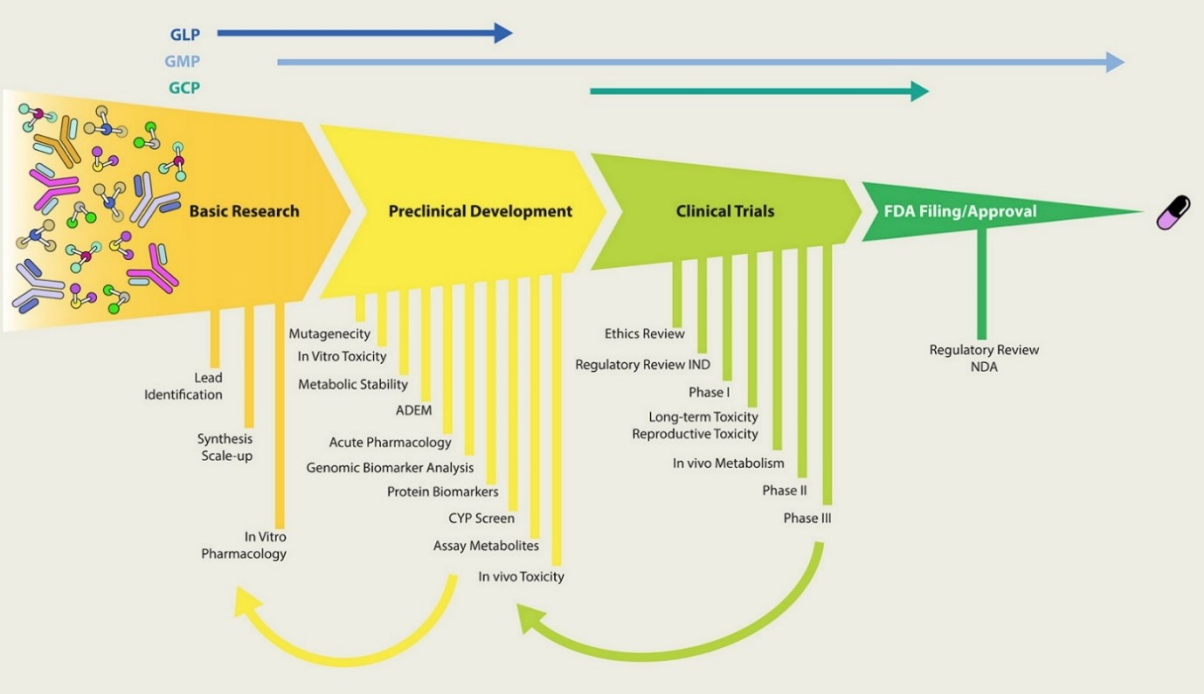

Figure 1: Outline of the steps involved in drug discovery and development. This scheme illustrates that although many substances are screened, only a small percentage will pass all the necessary steps involved in drug discovery, development and approval. Specific activities that occur during development stages are shown at the bottom of each stage. At the top, timelines for quality assurance guides are shown, which are good laboratory practices (GLP), good manufacturing practices (GMP) and good clinical practices (GCP) (1)

To minimize risk, the clinical development stage of the drug development process is designed to "fail fast and cheap" by quickly eliminating ineffective options. This highlights the importance of optimizing each step of the preclinical and clinical development process.(1,2)

The drug development process consists of five crucial steps, each containing several phases and stages. The phases involved in the development of a drug are [1] discovery, development and preclinical research, [2] clinical development, [3] regulatory approval and [4] post-marketing surveillance (4)

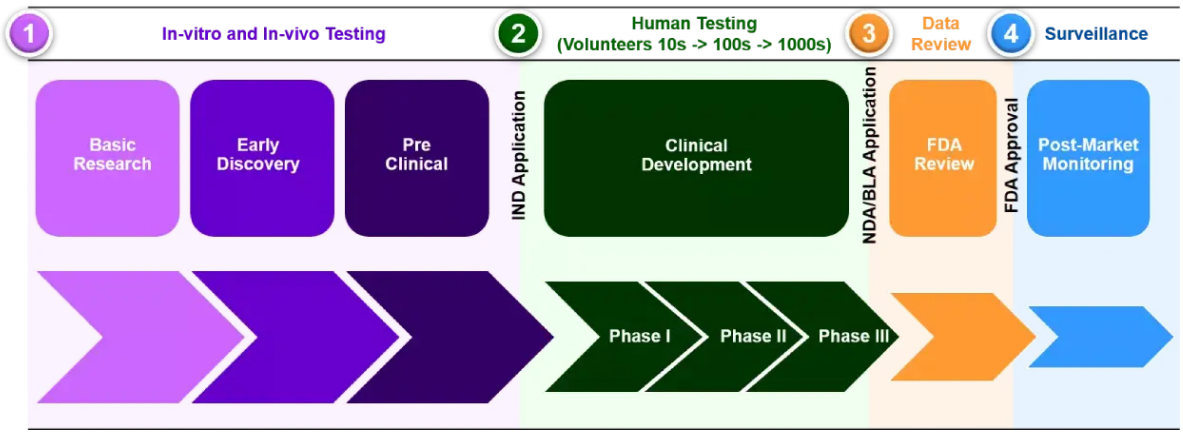

Figure 2: Overview of the stages involved in drug discovery and development. The first step is divided into three parts, the basic research, early discovery and preclinical research. Following the preclinical research, a new drug candidate undergoes clinical development, which consists of three phases. If clinical development is successful, the data gets reviewed for regulatory approval. After launching a new drug, it will be closely monitored to assure safety and further evaluate the efficacy.(4)

1.1.1 Early drug discovery

The objective of an early drug discovery program is to produce one or more clinical candidate molecules that have demonstrated biological activity against a disease-relevant target, as well as an acceptable level of safety and drug-like properties to justify human testing.

Conventional drug discovery approaches are impractical due to their high costs, failure rates, and lengthy processes. Therefore, researchers in the industry are constantly exploring new techniques and assessing emerging technologies from various fields.

There is no specific formula for producing a successful clinical candidate molecule, but collaboration between the fields of chemistry, biology, toxicology, and pharmacokinetics (PK) is a common approach in modern drug discovery programs. Among the modern technologies being heavily utilized are ultra-high-throughput drug screening and artificial intelligence. While traditional drug discovery relied mostly on natural sources for the development of medications, advances in science and technology have shifted the focus to small molecules. High-throughput screening and small-molecule drug libraries have revolutionized drug discovery. These methods serve as the starting point in drug discovery.

Once a target is identified, it needs to be fully validated through a multi-validation approach. The hit discovery process involves the development of compound screening assays to identify hit molecules, which are compounds that have desired activity and are confirmed upon retesting.

The hit to lead phase involves refining hit series to produce more potent and selective compounds with adequate pharmacokinetic properties. The final phase of drug discovery aims to improve lead compounds by maintaining favourable properties and addressing any deficiencies in the lead structure. Compounds that meet the goals of lead optimization and are ready for further characterization become preclinical candidates.

These molecules must have pharmacokinetic properties that allow for a predictable relationship between the drug dose and exposure. Central nervous system (CNS) targets are particularly complex because of the blood-brain barrier (BBB). Efficacy and toxicity, which are typically the cause of late lead failure, remain major challenges in the drug discovery field. The high attrition rate of compounds entering the clinical phase poses financial risks. To quickly eliminate ineffective options, the process is designed to “fail fast and cheap”. Advances in medicinal chemistry and biological PK modelling have helped reduce the number of molecules with unsatisfactory properties entering clinical development.(1–3)

1.1.2 Preclinical research and clinical development

After discovering a lead compound, the preclinical phase of drug development begins with in vivo research to assess the drug's safety and efficacy. Researchers analyse the following information about the drug: its absorption, distribution, metabolisation, and excretion, potential benefits and mechanisms of action, optimal dosage and administration route, side effects and adverse events, effects on gender, race, or ethnicity groups, and interaction with other treatments.

Toxicology studies in at least two non-human species are usually conducted to determine a safe dose range and provide information about efficacy, toxicity, and PK.

Different administration routes such as oral, topical, intravenous, and inhalation are used to target specific areas or achieve controlled release of the drug. However, physiological barriers in animals or humans can hinder drug delivery. To overcome this, drug delivery systems are developed to prevent the drug from interacting with healthy tissue while still being effective. Formulation optimization is an ongoing process in preclinical and clinical stages to ensure proper delivery of the drug at the right time and concentration.

After completing preclinical research, researchers proceed to clinical drug development, which involves conducting clinical trials and volunteer studies to refine the drug for human use. They are divided into three phases with the purpose to confirm the drug's efficacy and safety.

In Phase 1, the drug is tested on humans for the first time, using fewer than 100 volunteers. The researchers assess the drug's safety and how it affects the body's absorption, metabolism, and elimination, as well as any side effects, to determine safe dosage ranges.

Phase 2 involves assessing the drug's safety and efficacy in an additional 100-500 patients, who may receive a placebo, or a standard drug previously used for treatment. During this phase, the optimal dose strength is analysed, schedules are created, and adverse events and risks are recorded.

In Phase 3, 1,000-5,000 patients are enrolled to enable the development of medication labelling and instructions for proper drug use. The researchers determine pharmacodynamic (PD) biomarkers, conduct PK analysis, and develop and validate bioanalytical methods.(4)

1.1.3 Regulatory approval and post-marketing surveillance

To apply for admission, the relevant agency must be provided with preclinical and clinical assessment data, following a specific procedure with defined deadlines.

After approval, the molecule must be manufactured according to strict regulations governing purity and stability. Ultimately, the new medicine must gain acceptance in the medical community so that physicians and patients can be confident in administering the medicine to the appropriate patients, at the correct doses, and at the right time.

After the drug is authorized, the agency will monitor the product's safety by requiring the company to submit periodic safety update reports. Any reported adverse reactions must be collected and transmitted to the agency periodically. If the drug's safety is compromised, the agency has the right to withdraw the authorization.(1,4)

1.2 Bioavailability and pharmacokinetics

In the context of pharmaceuticals, bioavailability refers to the degree and speed at which a drug reaches its intended site of action within the body. This concept can be broken down into two components: the quantitative amount of the drug that reaches the site, and the kinetic rate at which it does so.

Pharmacokinetics is a subfield of pharmacology that focuses on the processes by which a drug is absorbed, distributed, metabolized, and excreted by the body following administration. This involves

both descriptive and mathematical approaches to understand how the body interacts with the drug, apart from its pharmacodynamic effects.

Biopharmaceutics is a discipline that examines the interplay between the biological aspects of an organism and the physical and chemical properties that govern the preparation and behaviour of drugs and medicinal agents. This includes studying the relationship between the physicochemical properties of a drug, the dosage form in which it is administered, and the route of administration, with respect to the extent and rate of systemic drug absorption.

Taken together, biopharmaceutics and pharmacokinetics form a unified approach to study the key steps involved in the delivery and metabolism of a drug within the body. These fields are essential for developing a comprehensive understanding of drug efficacy, safety, and overall pharmacological profile. (5)

1.2.1 ADME

The term ADME is an abbreviation that stands for a series of key processes involved in the pharmacokinetics of a drug, including absorption, distribution, metabolism, and excretion (See figure 3). In brief, absorption describes the movement of a drug from its site of entry into the bloodstream, distribution involves the reversible transfer of drug molecules to the extravascular compartment, metabolism refers to the conversion of drugs via biotransformation mediated by enzyme-catalysed chemical reactions, and excretion refers to the physical removal of the drug from the body.

Metabolism and excretion are often considered together as the process of drug elimination, while distribution, metabolism, and excretion may be collectively referred to as drug disposition. These processes are all essential to understanding the pharmacological profile of a drug, including its efficacy, safety, and potential for drug-drug interactions.(5)

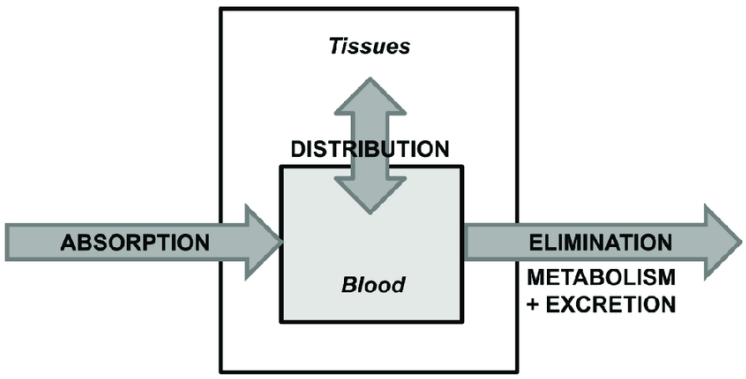

Figure 3: Scheme of the ADME process. This process includes absorption into the bloodstream, reversible distribution to extravascular compartments and elimination consisting of biotransformation or metabolism and excretion. (6)

1.2.1.1 Absorption

The process of absorption is a mass transfer phenomenon in which drug molecules move unchanged from the site of administration to the bloodstream. The rate and extent of drug absorption are influenced by a variety of factors, including the physicochemical properties of the drug, the pharmaceutical formulation used, and various anatomical and physiological factors. In many cases, the process of crossing epithelial or endothelial barriers is the rate-limiting step in drug absorption. This process involves overcoming a variety of biological barriers and surviving presystemic chemical or biochemical modifications.

It is important to note that drugs are typically not administered in their pure form, but rather as part of a pharmaceutical dosage form. To overcome biological barriers and achieve effective absorption, the drug must be in a free form, meaning it has been released from its pharmaceutical carrier and is in a solution. Some dosage forms may already provide the drug in solution, which can facilitate absorption. (5)

1.2.1.2 Distribution

Drug distribution refers to the movement of a drug from one location to another within the body. Once a drug is absorbed, it can enter the interstitial and intracellular spaces of different organs or tissues at varying levels and remain there for varying periods of time. This movement occurs through the endothelial lining of blood capillaries and can be influenced by binding to plasma proteins and tissue elements. It is important to note that only free, unbound drug molecules can efficiently cross endothelia and engage in the distribution process. Factors that affect drug distribution include physicochemical properties of the drug such as molecular weight, polarity, and degree of ionization, as well as physiological factors such as the expression levels and subcellular localization of drug transporters and tissue or organ perfusion. Additionally, the BBB can limit drug distribution, especially for molecules that are polar or have a high molecular weight. The movement of drugs across biological barriers can be classified as either perfusion rate-limited, blood flow-limited, or permeability rate-limited. Some drugs use active transport to move across biological barriers. (5)

1.2.1.3 Metabolism

In order to protect itself from exposure to potentially harmful substances, the body has developed various mechanisms to dispose metabolic waste. These mechanisms, which can also limit the bioavailability of therapeutic drugs, fall into three main categories: preventing non-physiological compounds from entering the bloodstream or sensitive organs, physically removing the compounds through urine, perspiration or respiration, and metabolizing them into drug metabolites that can be excreted more quickly than the parent compound. Drug biotransformation involves the enzyme-

mediated conversion of drugs into metabolites, usually in a sequential manner. These resulting metabolites are often inactivated from a pharmacological perspective but can also be active or toxic. The original substance may be excreted unchanged or as a metabolite, with all these possibilities often occurring simultaneously to contribute to the overall elimination of the drug.(5)

1.2.1.4 Excretion

Drug elimination, which encompasses both drug metabolism and excretion, is a vital process in the body's management of xenobiotic compounds and metabolic waste products. In some cases, drug metabolism is a necessary step for drug excretion, particularly for lipophilic drugs. The major excretion routes are through urine and bile. Compounds not reabsorbed in bile will ultimately be excreted in faeces. The kidneys and liver are specialized organs that have evolved to remove waste products and xenobiotics from the body, but other excretion routes include respiration, sweat, saliva, semen, hair, milk, and tears. The transport of drugs across various organs and tissues, as well as the systemic clearance, are critical to the excretion process. (5)

1.2.2 The blood-brain barrier

The blood-brain barrier is a crucial component of the CNS that acts as a gatekeeper and regulates the microenvironment of the brain. It is an intricate structure that performs several functions, including controlling molecular traffic to keep out toxins, maintaining ionic balance, separating central and peripheral neurotransmitter pools to minimize crosstalk, and facilitating immune surveillance and responsiveness with minimal inflammation. These functions are critical for proper brain cell function and for protecting neural tissue from harmful elements.

The blood vessels that vascularize the CNS have unique properties that enable them to regulate the movement of molecules, ions, and cells between the blood and the brain. This adjustment of homeostasis is crucial for the proper functioning of neurons and for the protection of the neural tissue. The BBB is particularly important for neurological diseases, as alterations to the barrier properties are a key factor in the development and progression of various conditions.

The core structure of the BBB is built of endothelial cells (ECs) that line the blood vessels. These cells are morphologically and functionally distinct from peripheral ECs and are held together by tight and adherens junctions, which limit the paracellular transport of solutes (See figure 4). The ECs of the CNS contain a variety of enzymes, that metabolize and inactivate metabolites. The ECs of the CNS also have higher numbers of mitochondria than peripheral ECs, reflecting a greater energy expenditure to drive ion gradients. Additionally, the ECs have a net negative surface charge and a lack of fenestrations, which prevents the rapid exchange of molecules between the blood and the brain. They also have very

low levels of leukocyte adhesion molecules, which restricts the number of immune cells that can enter the CNS.

The basement membrane is an acellular component of the BBB that provides stability for the cellular components and regulates their interactions. This membrane is also essential for endothelial cell polarization and for the proper localization of transporters and lumen formation.

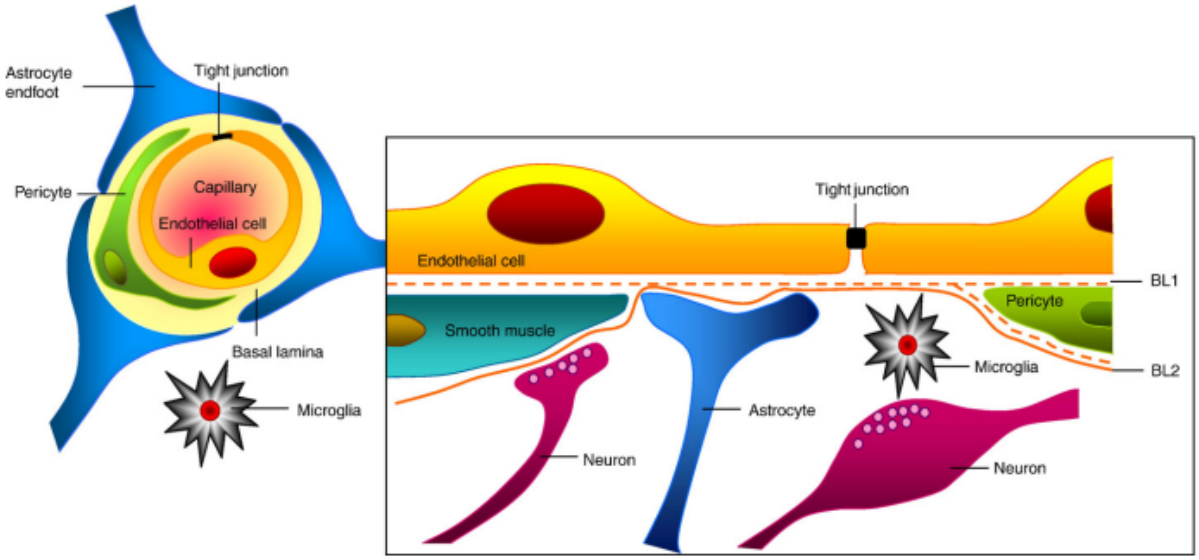

Figure 4: Schematic representation of the BBB. ECs line the blood vessel and are held together by tight junctions. The basement membrane provides stability and encloses smooth muscle and pericytes. Maintenance of the BBB is ensured by neurons, astrocytes and microglia. (7)

The BBB is a complex structure, that acts not just as a physical barrier, but also as a secretory body, metabolic barrier, and selective interface for the transport of molecules into the CNS. The regulation of molecular traffic at the BBB is crucial for maintaining the cerebral microenvironment and is a result of anatomical and biochemical properties.

The BBB presents a significant obstacle for delivering drugs to the CNS, making it difficult to develop effective treatments for CNS disorders. The BBB has a restrictive nature that prevents most small molecule drugs (98%) and almost all large-molecule therapeutics from reaching the brain. Efflux transporters further reduce the therapeutic concentration of lipophilic drugs in the brain, as well as the metabolism of xenobiotics by enzymes. Therefore, successfully delivering drugs to the brain requires tailored strategies, and overcoming the BBB is an essential consideration in the development of CNS-targeted therapeutics.(7–9)

1.2.3 Physicochemical properties

The properties of a drug, including its physical and chemical characteristics and molecular structure, have a significant impact on how it is processed in the body, its efficacy, and its safety. As a result,

current trends in drug development focus on examining both the properties of the drug and its ability to bind to its intended target. The idea of "drug-likeness" involves establishing appropriate limits for fundamental properties based on general guidelines to assist medicinal chemists in selecting promising drug candidates.

These guidelines consider key factors such as lipophilicity and molecular weight. As modern technologies produce more complex compounds, these properties become increasingly important in terms of bioavailability.(10)

The role of physicochemical properties of drugs has been a subject of study since the 1960s, when Hansch et al. conducted early research in this area.(11) The initial quantitative structure-activity relationship (QSAR) studies focused on lipophilicity, electronic properties, and steric properties as predictors of biological activity.(12) Over time, the field of QSAR has expanded significantly, with a shift in drug design strategy towards a more holistic approach that considers ADME properties and safety concerns in addition to target affinity. In order to increase the chances of success and reduce the rate of attrition, drug candidates should possess favourable physicochemical and molecular properties. The concept of drug-likeness, which is primarily concerned with pharmacokinetics and safety, provides a set of simple rules to guide chemical space exploration.(10)

Traditional physicochemical properties, such as lipophilicity, solubility, and ionization, are widely recognized as key factors in drug discovery. Lipophilicity is particularly crucial, as it can affect both the pharmacokinetic and pharmacodynamic properties of a drug, as well as its potential toxicity. High lipophilicity can lead to undesirable drug characteristics, including unpredictable metabolism, high plasma protein binding, and tissue accumulation. Conversely, aqueous solubility is critical for drug formulation and oral administration. (10) In fact, solubility within the physiological pH range, in combination with permeability, is a crucial parameter in the Biopharmaceutical Classification System (BCS), which classifies drugs into four categories. BCS is of great interest to the pharmaceutical industry, as drugs in class I (high solubility/high permeability) are exempt from bioequivalence studies. (13) Most drugs contain ionizable groups, with basic functions being the most common. While acidic functionality is essential in some cases as a receptor requirement, strongly acidic groups can be detrimental to permeability.

Molecular descriptors can be divided into two categories: those that can predict the biological activity of new compounds or screen compound libraries, and those that provide insight into the mechanism of action. In terms of receptor-ligand interactions, these involve electrostatic interactions, hydrogen bonding, van der Waals, and hydrophobic interactions. Electronic properties can be expressed by traditional electronic substituent constants, energy parameters, maximum or minimum electrostatic

potential, dipole moments, partial charges, and protonation states or ionization constants for acidic/basic groups. Hydrogen bonding is commonly described by the count of hydrogen bond acceptor and donor sites, hydrogen bond acidity and alkalinity parameters, and topological polar surface area (tPSA). Lipophilicity, molecular size, hydrogen bonding, tPSA, and flexibility are important properties for bioavailability and safety of drug candidates but can often conflict with receptor requirements. (10)

1.2.3.1 Ionization constant

The ionization constant, also referred to as the acid dissociation constant (pK_a), is a measure of the strength of an acid in solution. It is defined as the negative logarithm of the dissociation constant (K_a) of an acid. The pK_a represents the pH at which the concentration of ionized and unionized forms is equal and is used to describe the degree to which an acid dissociates (or ionizes) in water to form hydrogen ions (H^+) and its conjugate base. (14)

$$K_a = \frac{[H^+] \cdot [A^-]}{[HA]}$$

Equation 1: The equation for the ionization constant for a weak acid HA. K_a is the acid dissociation constant, $[H^+]$ is the concentration of hydrogen ions, $[A^-]$ is the concentration of the conjugate base of the acid, and [HA] is the concentration of the undissociated acid.

The Brønsted-Lowry theory is the most widely accepted and useful explanation of the ionization of acids and bases. This theory defines an acid as any substance that can donate a hydrogen ion, while a base is a substance that can accept a hydrogen ion. Strong acids and bases are completely ionized in the pH range of 0-14, while weaker acids and bases are only partially ionized in parts of this range. Brønsted was the first to demonstrate the benefit of having the ionization of both acids and bases expressed on a single scale, similar to the use of pH to indicate both alkalinity and acidity. (15)

It was in 1907 that Henderson first presented a paper detailing the correlation between the hydrogen ion $[H^+]$ and the composition of a buffer. It was not until 1916 that Hasselbalch proposed the well-known Henderson-Hasselbalch equation, which remains the most frequently used equation for calculating pK_a values. The Henderson-Hasselbalch equation can be used to estimate the ionized and unionized drug concentrations at a given pH.

$$pH = pK_a + \log \frac{[A^-]}{[HA]}$$

Equation 2: Henderson-Hasselbalch equation. The pH equals the negative logarithm of the hydrogen ion concentration in the solution, pK_a is the negative logarithm of the acid dissociation constant, $[A^-]$ is the concentration of the conjugate base of the acid, and [HA] is the concentration of the undissociated acid.

Despite being referred to as a constant, the ionization constant is not really a constant. It varies depending on temperature, ionic strength, and the dielectric constant of the solvent.

The pK_a is one of the most widely utilized physicochemical parameters, attracting attention from a diverse array of research areas. Both pH and pK_a play a crucial role in comprehending the behaviour of chemical substances. (16,17)

The ionization constant of a drug affects the drug's pharmacokinetics and pharmacodynamics. The absorption of drugs, that are primarily transported by passive diffusion, is greatly determined by the pK_a of the drug. Since most drugs are weak electrolytes, their degree of ionization is dependent on the pH of the biological fluid. For weak acids, the unionized form dominates at pH values lower than the pK_a, whereas for weak bases, the ionized form dominates. For example, at neutral pH, a drug with a low pK_a will be more ionized, while a drug with a high pK_a will be more unionized. This in turn affect its ability to penetrate biological membranes and reach its target.

In summary, the ionization constant plays a key role in determining the behaviour of a drug and is therefore a critical aspect to consider when assessing the potential of a compound. Knowing the pK_a of a drug can assist pharmaceutical chemists in refining its formulation and enhancing its therapeutic efficacy. (14)

1.3 Methodology of preclinical research

1.3.1 Computer-aided drug design

Computer-aided drug design (CADD) is a rapidly growing field that involves the use of computational methods to accelerate the drug discovery process. With the advancements in computational power and the availability of vast amounts of data, CADD has become an indispensable tool in the pharmaceutical industry for predicting drug efficacy and safety, and for screening large compound libraries.

One of the primary goals of CADD is to reduce the time and cost associated with the development of new drugs. Traditional drug discovery typically takes many years and costs billions of dollars. With CADD, researchers can use computer simulations to predict the binding of potential drug molecules

to target proteins, as well as to evaluate the PK properties of the compounds. This allows them to prioritize drug candidates before performing expensive and time-consuming laboratory experiments.

The CADD process involves several steps, including target identification and validation, compound library design, virtual screening, and hit optimization. Target identification involves the selection of a protein target that is involved in a specific disease, and the validation of the target's role in the disease. Once a target has been validated, compound libraries are designed, and virtual screening is performed to identify potential drug candidates that can bind to the target.

In virtual screening, large compound libraries are screened against the target protein using molecular docking simulations or machine learning algorithms. The most promising compounds are then optimized for potency, selectivity, and PK properties using repeated rounds of structural modifications and computational analysis. Finally, lead compounds are selected and tested in vitro and in vivo.

CADD methods can also be used to design drugs that target specific mutations or disease-causing mechanisms. For example, structure-based drug design can be used to design small molecules that bind to specific sites on mutated proteins, while fragment-based drug design can be used to design drugs that target protein-protein interactions or allosteric sites.

In addition to improving the efficiency of the drug discovery process, CADD can also help reduce the failure rate of drugs in clinical trials. By predicting the efficacy and safety of drugs before they are tested in humans, CADD can help identify potential issues and improve the chances of success in clinical trials.

In conclusion, CADD is a powerful tool for accelerating the drug discovery process, reducing costs, and improving the success rate of drug candidates. As the field continues to evolve, it is likely that CADD will play an increasingly important role in the development of new drugs to treat a wide range of diseases. (6,18)

1.3.2 CNS MPO score

Neurological drugs can take up to 18 years to complete the journey from laboratory evaluation to regulatory approval. (1) This has prompted the need for improving the survival of drug candidates and speeding up their identification. To achieve this, medicinal chemists use guiding principles, such as Lipinski's Rule of Five (Ro5), to design druglike compounds. (19) The original Ro5 for orally active substances outlines four basic physicochemical characteristics linked to 90% of orally administered drugs that have passed Phase II trials. According to the Ro5, drugs with a molecular weight exceeding 500 g/mol, a logP greater than 5, more than 5 hydrogen bond donors, or more than 10 hydrogen bond acceptors are prone to poor absorption and permeation. These parameters, which indicate favourable

aqueous solubility and intestinal permeability, play a crucial role in determining oral bioavailability. (20,21) However, it falls short of aligning all the desired ADME and safety attributes, especially regarding CNS-active drugs. This is where the central nervous system multiparameter optimization (CNS MPO) score comes into play. This algorithm assesses and balances the effects of multiple variables, weighted based on their importance, to provide greater flexibility in drug design and increase the odds of success.

The CNS MPO algorithm is based on six fundamental parameters and a variation of Harrington's optimization method. This approach evaluates the impact of multiple parameters without the limitations of strict cut-offs and expands the design space. The CNS MPO desirability score ranges from 0.0 to 6.0, with a score from 0.0 to 1.0 assigned to each of the six parameters. The algorithm provides an overall composite score, while individual scores still highlight potential problems that a compound may encounter (See table 1).

Table 1: Desirable and less desirable ranges of the six physicochemical properties, that are considered for the calculation of the CNS MPO score.

properties	weight	more desirable range	less desirable range
logP	1.0	logP ≤ 3	logP > 5
logD	1.0	logD ≤ 2	logD > 4
MW	1.0	MW ≤ 360	MW > 500
tPSA	1.0	40 < tPSA ≤ 90	tPSA ≤ 20; tPSA > 120
HBD	1.0	HBD ≤ 0.5	HBD > 3.5
pK_a	1.0	$pK_a \leq 8$	$pK_a > 10$

The CNS MPO algorithm offers several advantages over the use of single parameters or hard cut-offs. It provides a holistic assessment of a compound's ADME and safety attributes and improves the odds of identifying compounds with these attributes aligned in one molecule. The tool is simple to use and can be implemented using common software, such as Excel. It helps prioritize design ideas and triage high-throughput screening hits and facilitates the assessment of competitive intelligence in patent and literature databases.

In conclusion, the CNS MPO algorithm is a probabilistic tool that provides a holistic evaluation of druglike compounds and improves the odds of identifying successful candidates. It creates flexibility in design, expands the design space, and offers advantages over the use of single parameters or hard cut-offs. The algorithm can be used prospectively in design to reduce the number of cycles and speed up the identification of compounds with enhanced survival. (19,22)

1.3.3 Determination of the pK_a

The determination of the ionization constant is a critical step in drug discovery and development. It can inform decisions about the optimal state of charge for a drug candidate, its route of administration, and its dosing regimen, improving the chances of success in clinical trials. A compound's pK_a provides valuable information on the ionization state under different physiological conditions, which is essential for predicting the pharmacokinetic properties of the compound, such as solubility, permeability, and bioavailability. Several techniques are available for pK_a determination, including potentiometric titration, spectrophotometric titration, NMR spectroscopy, and others, each with its advantages and limitations. The choice of method should be carefully considered to ensure accurate and reliable results. (14,15,23)

1.3.3.1 Potentiometry

Potentiometric determination of the ionization constant is a widely used method to measure the ionization constant (pK_a) of a molecule. This method is based on the measurement of the potential difference between two electrodes immersed in a solution containing the molecule in a known concentration and at a specific pH.

In this method, a reference electrode and a glass electrode are used. The glass electrode contains a pH-sensitive glass membrane that responds to changes in H^+ concentration. The electrodes are connected to a high-impedance voltmeter or a pH meter.

To measure the ionization constant of the molecule, a solution of the drug in a buffer of known pH is prepared. The pH is adjusted to a value close to the expected pK_a of the drug. The two electrodes are then immersed in the solution, and the potential difference between the two electrodes is measured. The pH of the solution is then gradually changed by the addition of a strong acid or a strong base, and the potential difference is measured at each pH.

The pK_a of the drug is determined from the pH at which the ratio of the protonated and deprotonated forms of the drug is equal, which corresponds to the point where the potential difference between the two electrodes is zero. This is known as the inflection point of the titration curve.

The potentiometric determination of the ionization constant has several advantages over other methods. It is a non-destructive method, requires only small amounts of sample, and can be performed quickly and accurately. However, the method has some limitations. The presence of impurities or other ionizable species in the solution can interfere with the measurement, and the pH electrode may need to be calibrated before each use. (24,25)

1.3.3.2 Spectrophotometry

Spectrophotometric determination of the ionization constant is another commonly used method for determining the acidity or alkalinity of a compound. This method is based on the measurement of the absorbance or transmittance of light by a sample solution at different wavelengths. The principle of this method is based on the fact that ionization of a compound changes the spectral properties of the compound. As a result, the absorbance or transmittance of light changes as a function of pH.

In the spectrophotometric method, a UV-visible spectrophotometer is used to measure the absorbance or transmittance of light by a sample solution at different pH values. A buffer solution of known pH is added to the sample solution, and the absorbance or transmittance of light is measured at different wavelengths. A plot of absorbance or transmittance versus wavelength is then constructed, and the resulting spectrum is used to determine the ionization constant.

To determine the ionization constant, the UV-visible spectrum is analysed to identify the wavelengths at which the absorbance or transmittance changes as a function of pH. This can be done by comparing the spectra obtained at different pH values.

The pK_a of the compound can be calculated from the spectral data by fitting the absorbance or transmittance data to the Henderson-Hasselbalch equation.

The spectrophotometric method is useful for determining the ionization constant of compounds that absorb light in the UV-visible range. This method is highly sensitive and can be used for compounds present in low concentrations. However, the method requires a highly pure sample, and the presence of impurities can interfere with the measurement. Additionally, this method is only suitable for compounds that have distinct spectral properties that change with ionization. (25,26)

1.3.3.3 Calculation

The ionization constant of a compound can be calculated using various software programs. These programs use different algorithms and methods to predict pK_a values based on the molecular structure of the compound. Some commonly used software programs for pK_a prediction include ACD/pK_a, MarvinSketch, and ChemAxon. (27,28)

ACD/pK_a is a software program that uses a database of over 17,000 experimental pK_a values to predict the pK_a of a given compound. The program uses several molecular descriptors, including hydrogen bond donor and acceptor groups, electronegativity, and charge distribution, to generate a predictive model for the compound. The program also considers the pH of the solution and the temperature at which the experiment is conducted.(27,29,30)

MarvinSketch is a chemical drawing software that can be used to predict pK_a values of a compound based on its structure. The program uses a combination of machine learning and rule-based methods to predict the pK_a values. The algorithm used by MarvinSketch considers the molecular structure of the compound and its functional groups to generate a predictive model. The program also allows the user to specify the solvent conditions and temperature for the experiment.

ChemAxon is a software program that uses a range of computational methods to predict pK_a values based on the molecular structure of a compound. The program uses a combination of empirical and quantum chemical calculations to generate a predictive model. The method used by ChemAxon is based on the determination of the most stable protonation state of the molecule at a given pH and considers the solvent conditions and temperature. (27,28,31–33)

The accuracy of pK_a predictions can vary depending on the software program and the molecular structure of the compound being analysed. In general, software programs that use experimental data for their predictive models tend to be more accurate than those that use purely computational methods. It is also important to note that pK_a values can be influenced by several factors, including temperature, solvent conditions, and the presence of other compounds in the solution. Therefore, it is important to use caution when interpreting pK_a values. (27–29)

1.4 Standard operating procedures

A standard operating procedure (SOP) is a written document that outlines a set of instructions or procedures to be followed when carrying out a specific task or process. It is used to ensure consistency and quality in the performance of tasks and processes, and is a crucial component in many industries, including healthcare, manufacturing, and research.

SOPs provide detailed instructions on how to perform a task or process, including the materials and equipment required, the steps involved, and the expected outcomes. They often include safety precautions, quality control measures, and troubleshooting procedures in case of unexpected issues. SOPs can also provide guidance on record keeping, data analysis, and reporting.

SOPs are important for several reasons. They help to ensure consistency and accuracy in the performance of tasks, reducing the risk of errors or variability in results. They also promote safety, by providing clear instructions on the use of equipment and materials, as well as on any hazards or risks associated with the task. SOPs can also facilitate training, by providing a clear and structured outline of the steps involved in a task. (34)

2 Aim of this master thesis

The aim of this master thesis is to assess the fully automated SiriusT3 system for spectrophotometric and potentiometric pK_a determination. The study involved the measurement of pK_a values for 46 compounds, including BBB-penetrating, BBB non-penetrating, and compounds that interact with various efflux transporters.

One of the key physicochemical parameters that plays an important role in drug discovery and development is the ionization constant, or pK_a. Accurate determination of the pK_a is essential as it can have a significant impact on the pharmacokinetics and pharmacodynamics of a drug. Therefore, it is crucial to have reliable and accurate methods to measure it.

The main objectives of this project were to validate the accuracy and reproducibility of the measurements obtained using the SiriusT3 instrument and compare the results obtained from spectrophotometric and potentiometric measurement methods. Additionally, the calculated pK_a values were compared with the measured values to analyse the validity of a computational approach to pK_a determination. The results showed great discrepancies between experimental and predictive data, indicating the importance of experimental pK_a determination.

In addition to validating the instrument, this master thesis also aimed to establish a standard operating procedure for the SiriusT3 instrument and software for pK_a determination. The SOP provides a comprehensive manual for the characterization of compounds, which will be useful for future researchers working with the SiriusT3 instrument.

Finally, to investigate the relevance of the pK_a in predicting the blood-brain barrier penetration of compounds, this study analysed a set of 46 compounds and investigated the correlation between the ionization state at physiological conditions and BBB permeation.

The overall aim of this thesis is to provide a better understanding of the importance of pK_a determination in the drug discovery and development process and to reinforce the relevance of the ionization constant as a crucial physicochemical parameter. This work also demonstrates the potential of the fully automated SiriusT3 instrument as a tool for the accurate and rapid measurement of pK_a values.

3 Materials and methods

3.1 Equipment

For all measurements of this master thesis the SiriusT3 instrument and the corresponding software SiriusT3Control and SiriusT3Refine (Pion Inc., Billerica, USA) were used to assess and analyse the ionization constant of the sample compounds. The SiriusT3 instrument consists of a dispenser module, a titrator module and an autoloader module and the pK_a values were measured by a combination of automated potentiometric and UV-spectroscopic titration.

3.2 Reagents preparation

The reagents required to operate the SiriusT3 were prepared following the instructions of the user manual provided by Pion Inc. First, the ionic strength adjusted (ISA) water was prepared using 11.18 g ± 0.1 g potassium chloride (CAS: 7447-40-7, Sigma Aldrich) per litre of purified water to obtain a 0.15 M KCl solution. For the preparation of the base a potassium hydroxide ampoule (Tritisol®, CAS: 1310-58-3, Sigma Aldrich) was used to achieve a 0.5 M solution in purified water. To standardize the base titrant high purity potassium hydrogen phthalate (≥99.95%, CAS: 877-24-7, Sigma Aldrich) was used. The titration reagent of ISA methanol was created using 80% methanol (≥99.9%, CAS: 67-56-1, Sigma Aldrich) and 20% ISA water. The phosphate buffer for UV-metric pK_a analysis was prepared using 0.50 g ± 0.02 g anhydrous di-potassium hydrogen orthophosphate (CAS: 7785-11-4, Sigma Aldrich) per 200 mL ISA water. For the preparation of the acid titrant 49 mL HCl (≥37%, CAS: 7647-01-0, Sigma Aldrich) per litre of purified water were used to obtain a 0.5 M HCl solution. Remaining buffer solutions, including Fast UV buffer (Pion Inc. T1404007) and pH 7.00 buffer solution (Certipur®, Sigma Aldrich) were purchased ready-made. The surfactant and solvent wash solutions were freshly prepared as part of the daily maintenance. The surfactant wash solution consisted of 0.5% Triton® X-100 (CAS: 9036-19-5, Sigma Aldrich) and the solvent wash was a 50% 2-propanol (≥99.8%, CAS: 67-63-0, Sigma Aldrich) solution, both diluted with purified water. The purified water was drawn from an in-house water purification system (LaboStar® 10 RO DI System, Evoqua Water Technologies LLC, Pittsburgh, USA).

3.3 Sample preparation

The compounds were either purchased from ABX (Advanced Biomedical Compounds, Radeberg, Germany) or Sigma Aldrich (St. Louis, Missouri, USA). Information on all the measured samples, including the CAS numbers or product numbers and company is listed in table 2 and table 3.

For the UV-metric and Fast-UV measurements the compounds were solved in dimethyl sulfoxide (99.8%, CAS: 67-68-05, Sigma Aldrich) to create a stock solution with a concentration of 10 mM. The

sample solutions for the UV-metric measurements were topped with 25 µL phosphate buffer. For the potentiometric measurements 0.7 - 1.0 mg of each substance was weighed into a vial. When setting up the measurement the sample weight needs to be added to the SiriusT3Control software before running the assay, therefore the exact weight was noted down. All compounds were weighed using a Secura225D-1S weighing scale by Santorius.

Table 2: Compounds purchased from Sigma Aldrich with respective IUPAC names and CAS number.

IUPAC name	Trivial name	CAS number
(3R,5R)-7-[2-(4-fluorophenyl)-3-phenyl-4-(phenylcarbamoyl)-5-propan-2-ylpyrrol-1-yl]-3,5-dihydroxyheptanoic acid	Atorvastatin	134523-00-5
N-[(E)-[10-[(E)-(4,5-dihydro-1H-imidazol-2-ylhydrazinylidene)methyl]anthracen-9-yl]methylideneamino]-4,5-dihydro-1H-imidazol-2-amine	Bisantrene	78186-34-2
1-cyclohexyloxycarbonyloxyethyl 3-[[4-[2-(1-ethyltetrazol-5-yl)phenyl]phenyl]methyl]-2-oxo-1H-benzimidazole-4-carboxylate	Candesartan cilexetil	145040-37-5
4-[5-(4-methylphenyl)-3-(trifluoromethyl)pyrazol-1-yl]benzenesulfonamide	Celecoxib	169590-42-5
2-[2-[4-[(4-chlorophenyl)-phenylmethyl]piperazin-1-yl]ethoxy]acetic acid	Cetirizine	83881-51-0
6-chloro-3-[1-[3-(2-oxo-3H-benzimidazol-1-yl)propyl]piperidin-4-yl]-1H-benzimidazol-2-one	Domperidone	57808-66-9
(5S,5aR,8aR,9R)-5-[[(2R,4aR,6R,7R,8R,8aS)-7,8-dihydroxy-2-methyl-4,4a,6,7,8,8a-hexahydropyrano[3,2-d][1,3]dioxin-6-yl]oxy]-9-(4-hydroxy-3,5-dimethoxyphenyl)-5a,6,8a,9-tetrahydro-5H-[2]benzofuro[6,5-f][1,3]benzodioxol-8-one	Etoposide	33419-42-0
4-ethyl-3-methyl-N-[2-[4-[(4-methylcyclohexyl)carbamoylsulfamoyl]phenyl]ethyl]-5-oxo-2H-pyrrole-1-carboxamide	Glimepiride	93479-97-1

6-chloro-1,1-dioxo-3,4-dihydro-2H-1lambda6,2,4-benzothiadiazine-7-sulfonamide	Hydrochlorothiazide	58-93-5
8-[(3R)-3-aminopiperidin-1-yl]-7-but-2-ynyl-3-methyl-1-[(4-methylquinazolin-2-yl)methyl]purine-2,6-dione	Linagliptin	668270-12-0
(2S)-N-[(2S,4S,5S)-5-[[2-(2,6-dimethylphenoxy)acetyl]amino]-4-hydroxy-1,6-diphenylhexan-2-yl]-3-methyl-2-(2-oxo-1,3-diazinan-1-yl)butanamide	Lopinavir	192725-17-0
[2-butyl-5-chloro-3-[[4-[2-(2H-tetrazol-5-yl)phenyl]phenyl]methyl]imidazol-4-yl]methanol	Losartan	114798-26-4
1-[2-(2,4-dichlorophenyl)-2-[(2,4-dichlorophenyl)methoxy]ethyl]imidazole	Miconazole	22916-47-8
(2R,3S)-5-[3-(tert-butylamino)-2-hydroxypropoxy]-1,2,3,4-tetrahydronaphthalene-2,3-diol	Nadolol	42200-33-9
(3S,4aS,8aS)-N-tert-butyl-2-[(2R,3R)-2-hydroxy-3-[(3-hydroxy-2-methylbenzoyl)amino]-4-phenylsulfanylbutyl]-3,4,4a,5,6,7,8,8a-octahydro-1H-isoquinoline-3-carboxamide	Nelfinavir	159989-64-7
5-O-[2-[benzyl(methyl)amino]ethyl] 3-O-methyl 2,6-dimethyl-4-(3-nitrophenyl)-1,4-dihydropyridine-3,5-dicarboxylate	Nicardipine	55985-32-5
N-[4-(5-methyl-3-phenyl-1,2-oxazol-4-yl)phenyl]sulfonylpropanamide	Parecoxib	198470-84-7
4-N-(6-chloro-2-methoxyacridin-9-yl)-1-N,1-N-diethylpentane-1,4-diamine	Quinacrine	69-05-6

(S)-[(2R,4S,5R)-5-ethenyl-1-azabicyclo[2.2.2]octan-2-yl]-(6-methoxyquinolin-4-yl)methanol	Quinidine	56-54-2
(E)-1-N'-[2-[[5-[(dimethylamino)methyl]furan-2-yl]methylsulfanyl]ethyl]-1-N-methyl-2-nitroethene-1,1-diamine	Ranitidine	66357-59-3
2-ethoxy-4-[2-[[(1S)-3-methyl-1-(2-piperidin-1-ylphenyl)butyl]amino]-2-oxoethyl]benzoic acid	Repaglinide	135062-02-1
[9-(2-carboxyphenyl)-6-(diethylamino)xanthen-3-ylidene]-diethylazanium	Rhodamine 123	62669-70-9
1,3-thiazol-5-ylmethyl N-[(2S,3S,5S)-3-hydroxy-5-[[(2S)-3-methyl-2-[[methyl-[(2-propan-2-yl-1,3-thiazol-4-yl)methyl]carbamoyl]amino]butanoyl]amino]-1,6-diphenylhexan-2-yl]carbamate	Ritonavir	155213-67-5
N-[4-[1-hydroxy-2-(propan-2-ylamino)ethyl]phenyl]methanesulfonamide	Sotalol	959-24-0
(8S,9R,10S,11S,13S,14S,16R,17S)-9-fluoro-11,16,17-trihydroxy-17-(2-hydroxyacetyl)-10,13-dimethyl-6,7,8,11,12,14,15,16-octahydrocyclopenta[a]phenanthren-3-one	Triamcinolone	124-94-7

Table 3: Compounds purchased from ABX with respective IUPAC names and product number.

IUPAC name	**Trivial name**	**Product number**
2-fluoroethyl (1R,2S,3S,5S)-3-(4-iodophenyl)-8-methyl-8-azabicyclo[3.2.1]octane-2-carboxylate	2-FE-Beta-CIT	4150.0005
3-[2-[4-(4-fluorobenzoyl)piperidin-1-yl]ethyl]-2-sulfanylidene-1H-quinazolin-4-one	Altanserin	1810.001

methyl (1R,2S,3S,5S)-3-(4-iodophenyl)-8-methyl-8-azabicyclo[3.2.1]octane-2-carboxylate	Beta-CIT	4030.0003
methyl (1R,2S,3S,5S)-8-(3-(18F)fluoranylpropyl)-3-(4-iodophenyl)-8-azabicyclo[3.2.1]octane-2-carboxylate	Beta-CIT-FP	4130.0005
2-[1-[6-[2-fluoroethyl(methyl)amino]naphthalen-2-yl]ethylidene]propanedinitrile	DMFEAN	5030.0005
ethyl 3-[(1R)-1-phenylethyl]imidazole-4-carboxylate	Etomidate	1770.0005
3-(2-fluoroethyl)-8-[4-(4-fluorophenyl)-4-oxobutyl]-1-phenyl-1,3,8-triazaspiro[4.5]decan-4-one	FESP	1591.0005
5-bromo-N-[[(2S)-1-ethylpyrrolidin-2-yl]methyl]-2,3-dimethoxybenzamide	FLB457	1540.0005
6-[4-((^{18}F)fluoranylmethylsulfanyl)phenyl]-1,2,3,5,6,10*b*-hexahydropyrrolo[2,1-a]isoquinoline	(+)-FMe-McN 5652	4381.0005
1-fluoro-3-(2-nitroimidazol-1-yl)propan-2-ol	FMISO	1410.0005
1-[1-[4-(4-fluorophenyl)-4-oxobutyl]piperidin-4-yl]-3-methylbenzimidazol-2-one	FNMB	2760.0005
(E)-but-2-enedioic acid;methyl-4-[2-(3,4-dichlorophenyl)acetyl]-3-(pyrrolidin-1-ylmethyl)piperazine-1-carboxylate	GR-89696 fumarate	2070.0005
(6S,10bR)-6-(4-methylsulfanylphenyl)-1,2,3,5,6,10b-hexahydropyrrolo[2,1-a]isoquinoline	(+)-McN-5652	4370.0005
methyl 3-(1-phenylethyl)imidazole-4-carboxylate	Metomidate	1760.0005

(1S,2S,13R,21R)-22-(cyclopropylmethyl)-11-methyl-14-oxa-11,22-diazaheptacyclo[13.9.1.01,13.02,21.04,12.05,10.019,25]pentacosa-4(12),5,7,9,15,17,19(25)-heptaene-2,16-diol	N-Methylnaltrindole	2810.0005
2-[6-chloro-2-[4-(3-fluoropropoxy)phenyl]imidazo[1,2-a]pyridin-3-yl]-N,N-diethylacetamide	PBR 111	1656.001
methyl (1R,2S,3S,5S)-8-[(E)-3-iodoprop-2-enyl]-3-(4-methylphenyl)-8-azabicyclo[3.2.1]octane-2-carboxylate	PE2I	4160.0005
(4aR,10bR)-4-propyl-2,3,4a,5,6,10b-hexahydrobenzo[h][1,4]benzoxazin-9-ol;hydrochloride	(+)-PHNO HCl	1645.002
N-butan-2-yl-1-(2-chlorophenyl)-N-methylisoquinoline-3-carboxamide	PK 11195	1611.0005
3,5-dichloro-N-[[(2S)-1-ethylpyrrolidin-2-yl]methyl]-2-hydroxy-6-methoxybenzamide	Raclopride	1520.0005
(5R)-8-chloro-3-methyl-5-phenyl-1,2,4,5-tetrahydro-3-benzazepin-7-ol;hydrochloride	(-)-SCH23390 HCl	1466.0005

3.4 pK_a measurement

For the pK_a validation project all 46 sample measurements were performed with the fully automated SiriusT3 and the associated SiriusT3Control Software, using standard default settings and following the recommended instructions given in the user manual provided by Pion Inc. The SiriusT3 operates under an inert atmosphere, therefore all reagents and samples were degassed through a constant flow of Argon. All measurements were done in triplicates. For all compounds the psK_a was also measured using a methanol/water cosolvent mix.

3.4.1 Potentiometric measurements

The pH-metric measurements were performed using the SiriusT3 instrument, which utilizes a glass Ag/AgCl combination pH electrode to measure the pH of the solution. The pH-metric pK_a assay was designed using the SiriusT3Control software. Prior to the addition of the sample, a blank assay was performed to characterize the pH electrode and derive a titration curve.

The Sample Dissolution method was used to solubilize the test compounds in the assay medium at a pH where the sample is most soluble. Turbidity was monitored by a turbidity sensor to detect precipitation during the titration.

3.4.2 Spectrophotometric measurements

For the spectrophotometric measurements with the SiriusT3 system, two different methods, the Fast UV pK_a measurement and the UV-metric pK_a measurement, were employed. The SiriusT3 instrument used a deuterium lamp to measure the UV/Vis absorbance spectrum of the solution at each pH point recorded. This data was then displayed as a three-dimensional matrix of pH, absorbance, and wavelength data, which was then evaluated mathematically using the Beer-Lambert law and Target Factor Analysis (TFA).

For the Fast UV pK_a measurements a neutral linear buffer system was used, which allowed greater control of the pH during the titration. This enabled a fast and reliable change of pH, which did not require a stability time. As a result, a standard 40–50-point titration took less than 6 minutes.

For the UV-metric pK_a measurements a buffer was used to better control the pH during the titration. To record a stable reading, a latent period for the electrode was needed, which resulted in a standard 40–50-point titration that took approximately 20-25 minutes.

In both methods, turbidity was monitored by a turbidity sensor to ensure accurate measurements.

3.5 Data refinement

The subsequent data refinement of the measured aqueous ionization constant was performed using the SiriusT3Refine Software. The refinement to minimize differences between the experimental data and the mathematical model is done automatically by the SiriusT3Refine Software. The mathematical model included a set of mass and charge balance equations that modelled the equilibrium processes involved in the titration. The parameters in the mathematical model, including the sample pK_a and concentration, were varied in a stepwise fashion until the differences between the experimental data and the theoretical model were minimized. To determine the aqueous pK_a values of the test compounds the software utilized two methods. The first method was the Yasuda-Shedlovsky extrapolation, which plotted the cosolvent psK_a plus the log of water concentration against the reciprocal of the dielectric constant of the medium. The second method was the linear extrapolation. For further analysis , this study employed the results from the Yesuda-Shedlovsky extrapolation.

3.6 Sketching and calculations

All structures of the 46 tested compounds were drawn with Chemicalize and Marvin Sketch (© 1998-2022 Chemaxon Ltd., Budapest, Hungary). The calculation of the ionisation constant was performed using Chemicalize Software and the calculation of the CNS MPO score was performed using MarvinSketch.

3.7 Graphical Analysis

All graphs and diagrams were created using Microsoft ® Excel Version 16.67.

4 Results and discussion

The primary aim of this master thesis project was to determine the ionization constants of a diverse set of 46 compounds using three different methods: pH-metric, Fast UV, and UV-metric. The samples were divided into three categories.

1. Compounds known to be BBB-penetrating.
2. Compounds known to be BBB non-penetrating.
3. Compounds known to show interaction with various efflux transporters.

The following sections presents the results of the pK_a determination obtained through each method, as well as a comparison of their accuracy. Due to the limited availability of some compounds, only 21 were tested with the pH-metric method, while all 46 compounds were measured with the Fast UV and UV-metric methods.

The results demonstrate that using the SiriusT3 instrument and software is a reasonable approach for accurate and efficient pK_a determination, with each method having its own strengths and limitations. Supporting data to illustrate the accuracy and precision of the measurements is provided, as well as potential sources of error that need to be considered when interpreting the results.

4.1 Evaluation of the SiriusT3 system

The tables presented in this section provide a comprehensive summary of the pK_a values obtained through UV-metric, Fast UV, and pH-metric methods. Each table contains the mean and standard deviation (SD) of the triplicate measurements for each compound, as well as the calculated pK_a values. These tables provide a detailed overview of the experimental results, allowing for easy comparison and analysis of the data.

The use of triplicate measurements ensured the reliability, reproducibility and accuracy of the results, while the inclusion of mean and SD values provide a measure of the experimental error. The information presented in these tables is crucial for the subsequent discussion of the results and the conclusions that are drawn from them.

*Table 4: pK_a values for 20 compounds known to be BBB penetrating, obtained through Fast UV, UV-metric and pH-metric methods using the SiriusT3 system. Table includes mean and SD from triplicate (n=3) measurements and the corresponding calculated pK_a values. *n=2 **n=1.*

Compound	**Measurement method**		**pk_a**			
			Measured		**Calculated**	
					Chemi-calize	**Marvin Sketch**
2-FE-Beta-CIT	Fast UV	pK_a	9.52 ± 0.034		13.42	9.38
		psK_a	9.66 ± 0.060			
	UV-metric	pK_a	9.40 ± 0.055			
		psK_a	9.19 ± 0.040			
Altanserin	Fast UV	pK_a	7.55 ± 0.006	8.94 ± 0.007	6.74 8.27	6.74 8.27
		psK_a	7.45 ± 0.040	8.92 ± 0.010		
	UV-metric	pK_a	7.85 ± 0.065	8.31 ± 0.166		
		psK_a	7.57 ± 0.020	8.84 ± 0.030		
Beta-CIT	Fast UV	pK_a	9.71 ± 0.047		13.50	9.46
		psK_a	9.77 ± 0.020			
	UV-metric	pK_a	9.69 ± 0.045			
		psK_a	8.89*			
Beta-CIT-FP	Fast UV	pK_a	9.41 ± 2.250		13.76	9.72
		psK_a	9.54 ± 0.040			
	UV-metric	pK_a	9.17 ± 0.084			
		psK_a	9.30 ± 0.110			
DMFEAN	Fast UV	pK_a	2.13 ± 0.135		2.58	2.58
		psK_a	2.20 ± 0.460			
	UV-metric	pK_a	2.27 ± 0.064			
		psK_a	2.59 ± 0.010			
Etomidate	Fast UV	pK_a	4.19 ± 0.008		4.25	4.25
		psK_a	4.13 ± 0.040			
	UV-metric	pK_a	4.24 ± 0.023			
		psK_a	4.32 ± 0.000			
FESP	Fast UV	pK_a	8.37 ± 0.070		7.74	4.02 7.74
		psK_a	8.59 ± 0.010			
	UV-metric	pK_a	8.25 ± 0.016			
		psK_a	8.42 ± 0.030			
FLB 457	Fast UV	pK_a	9.02 ± 0.044		9.07	9.07
		psK_a	9.06 ± 0.000			
	UV-metric	pK_a	8.98 ± 0.010			
		psK_a	8.98 ± 0.030			
	pH-metric	pK_a	9.05 ± 0.010			

(+)-FMe-McN 5652	Fast UV	pK_a	10.64 ± 0.038		8.64	10.34
		psK_a	3.46 ± 0.610			
	UV-metric	pK_a	6.47 ± 0.109			
		psK_a	7.11*			
FNMB	Fast UV	pK_a	8.50 ± 0.034		6.75	7.85
		psK_a	8.32 ± 0.120			
	UV-metric	pK_a	8.27 ± 0.145			
		psK_a	8.39 ± 0.070			
GR-89696 fumarate	Fast UV	pK_a	8.30 ± 0.103		8.63	2.78 8.63
		psK_a	7.69 ± 0.150			
	UV-metric	pK_a	8.48 ± 0.045			
		psK_a	7.93*			
	pH-metric	pK_a	8.67 ± 0.040			
(+)-McN-5652	Fast UV	pK_a	7.74 ± 0.090		8.67	10.37
		psK_a	8.78 ± 0.110			
	UV-metric	pK_a	8.66 ± 0.131			
		psK_a	8.42 ± 0.340			
Metomidate	Fast UV	pK_a	4.15 ± 0.011		4.25	4.25
		psK_a	4.07 ± 0.070			
	UV-metric	pK_a	4.21 ± 0.033			
		psK_a	4.20*			
N-Methylnaltrindole	Fast UV	pK_a	8.67 ± 0.004	9.94 ± 0.028	7.62 9.22	7.91 9.24
		psK_a	9.15 ± 0.020	10.03 ± 0.070		
	UV-metric	pK_a	8.68 ± 0.014	9.92 ± 0.008		
		psK_a	8.96 ± 0.008	9.77 ± 0.000		
PBR 111	Fast UV	pK_a	4.84 ± 0.118		5.05	2.57 5.08
		psK_a	5.07 ± 0.030			
	UV-metric	pK_a	4.80 ± 0.099			
		psK_a	5.11 ± 0.000			
PE2I	Fast UV	pK_a	9.23 ± 0.191		13.29	9.27
		psK_a	8.89 ± 0.060			
	UV-metric	pK_a	8.31 ± 0.311			
		psK_a	8.86 ± 0.030			
(+)-PHNO HCl	Fast UV	pK_a	7.25**	9.86**	7.11 9.68	7.11 9.68
		psK_a	7.75**	10.81**		
	UV-metric	pK_a	7.74 ± 0.138	9.82 ± 0.004		
		psK_a	7.70 ± 0.280	10.01 ± 0.030		
	pH-metric	pK_a	7.37*	9.73*		
PK 11195	Fast UV	pK_a	1.69 ± 0.044		0.88	0.80 1.07
		psK_a	1.20 ± 0.280			
	UV-metric	pK_a	1.46 ± 0.015			
		psK_a	2.28*			
Raclopride	Fast UV	pK_a	6.04 ± 0.008	9.58 ± 0.038	6.76	6.76

		psK_a	6.26 ± 0.010	9.56 ± 0.080	9.07	9.07
	UV-metric	pK_a	6.00 ± 0.037	9.59 ± 0.017		
		psK_a	6.11 ± 0.040	9.72 ± 0.030		
(-)-SCH23390 hydrochloride	Fast UV	pK_a	7.94 ± 0.154	9.82 ± 0.877	8.24 9.26	8.24 9.26
		psK_a	7.87 ± 0.410	8.37 ± 2.700		
	UV-metric	pK_a	7.80 ± 0.020	9.52 ± 0.788		
		psK_a	7.23 ± 1.380	9.30 ± 2.440		
	pH-metric	pK_a	6.72*	9.75*		

*Table 5: pK_a values for 12 compounds known to be BBB non-penetrating, obtained through Fast UV, UV-metric and pH-metric methods using the SiriusT3 system. Table includes mean and SD from triplicate (n=3) measurements and the corresponding calculated pK_a values. *n=2 **n=1.*

Compound	**Measurement method**		**pk_a**				
			Measured			**Calculated**	
						Chemi-calize	**Marvin Sketch**
Candesartan cilexetil	Fast UV	pK_a		3.36 ± 0.150	6.05 ± 0.062	1.50 3.51 5.85	1.45 4.23
		psK_a	2.04 ± 0.070	4.34 ± 0.040			
	UV-metric	pK_a	1.01 ± 0.340	4.76 ± 0.215	6.56 ± 0.387		
		psK_a	1.98 ± 0.010	4.27 ± 0.020			
Celecoxib	Fast UV	pK_a	9.54 ± 0.003			10.60	10.60
		psK_a	9.69 ± 0.000				
	UV-metric	pK_a	9.45 ± 0.000				
		psK_a	9.36*				
Cetirizine	Fast UV	pK_a	2.47 ± 0.179	7.99 ± 0.048		3.01 3.77 7.97	2.97 3.76 7.97
		psK_a	2.30*	7.96*			
	UV-metric	pK_a	2.36 ± 0.130	7.96 ± 0.052			
		psK_a	2.68*	8.04*			
	pH-metric	pK_a	2.91*	8.06*			
		psK_a	3.16 ± 0.240	8.07 ± 0.050			
Domperidone	Fast UV	pK_a	6.32 ± 0.144	11.07 ± 0.038		5.83 12.72	8.03 12.72
		psK_a	8.22 ± 0.130	11.07 ± 0.030			
	UV-metric	pK_a	7.32 ± 0.075	11.56 ± 0.160			
		psK_a	7.78 ± 0.090	11.07 ± 0.070			
FMISO	Fast UV	pK_a	12.19 ± 0.309			13.64	13.64
		psK_a	12.04 ± 0.310				
	UV-metric	pK_a	11.60 ± 0.316				
		psK_a	12.09 ± 0.130				

HCT	Fast UV	pK_a	8.74 ± 0.009	9.99 ± 0.004	9.09 9.83	9.57 10.28
		psK_a	8.87 ± 0.020	10.19 ± 0.020		
	UV-metric	pK_a	8.73 ± 0.003	9.97 ± 0.008		
		psK_a	8.79 ± 0.040	10.03 ± 0.050		
	pH-metric	pK_a	8.89 ± 0.040	10.27 ± 0.040		
		psK_a	8.86 ± 0.090	10.00 ± 0.180		
Linagliptin	Fast UV	pK_a	1.88 ± 0.003	8.73 ± 0.011	3.01 9.86	3.01 9.86
		psK_a	1.78 ± 0.040	8.63 ± 0.020		
	UV-metric	pK_a	1.94 ± 0.010	8.72 ± 0.011		
		psK_a	1.65 ± 0.130	8.62 ± 0.010		
	pH-metric	pK_a		8.76 ± 0.010		
		psK_a		8.15*		
Miconazole	Fast UV	pK_a	5.26 ± 1.124		6.48	6.48
		psK_a	7.19*			
	UV-metric	pK_a	5.55 ± 1.047			
		psK_a	7.58*			
	pH-metric	pK_a	3.58 ± 0.040			
		psK_a	6.17*			
Nadolol	Fast UV	pK_a	9.81 ± 0.083		9.36	9.36
		psK_a	10.85 *			
	UV-metric	pK_a	9.89 ± 0.067			
		psK_a	9.41 ± 0.050			
	pH-metric	pK_a	9.84 ± 0.010			
		psK_a	9.87 ± 0.020			
Parecoxib	Fast UV	pK_a	4.51 ± 0.005		5.54	5.54
		psK_a	4.75 ± 0.001			
	UV-metric	pK_a	4.52 ± 0.007			
		psK_a	4.63 ± 0.001			
	pH-metric	pK_a	5.18 ± 0.030			
		psK_a	4.71 ± 0.040			
Repaglinide	Fast UV	pK_a	3.82 ± 0.008	6.18 ± 0.021	3.50 5.39	1.90 3.52 5.39
		psK_a	4.26 ± 0.030	5.75 ± 0.450		
	UV-metric	pK_a	3.82 ± 0.005	6.21 ± 0.009		
		psK_a	4.53 ± 0.490	6.08 ± 0.720		
	pH-metric	pK_a	3.85*	6.46*		
		psK_a	4.43 ± 0.200	5.70 ± 0.090		
Sotalol	Fast UV	pK_a	8.24 ± 0.005	9.73 ± 0.04	8.75 9.64	8.75 9.64
		psK_a	8.53 ± 0.040	9.45 ± 0.06		
	UV-metric	pK_a	8.23 ± 0.001	9.65 ± 0.006		
		psK_a	8.18**	9.60**		
	pH-metric	pK_a	8.33*	10.01*		
		psK_a	8.32 ± 0.000	9.14 ± 0.160		

*Table 6: pK_a values for 14 compounds known to show interactions with various efflux transporters, obtained through Fast UV, UV-metric and pH-metric methods using the SiriusT3 system. Table includes mean and SD from triplicate (n=3) measurements and the corresponding calculated pK_a values. *n=2 **n=1.*

Compound	**Measurement method**		**pk_a**			
			measured		**Calculated**	
					Chemi-calize	**Marvin Sketch**
Atorvastatin	Fast UV	pK_a	4.73 ± 0.092		4.31	4.31
		psK_a	n.e.			
	UV-metric	pK_a	4.50 ± 0.102			
		psK_a	n.e.			
	pH-metric	pK_a	4.55 ± 0.020			
		psK_a	n.e.			
Bisantrene	Fast UV	pK_a	7.43 ± 0.005		6.62 7.22	5.61 6.21
		psK_a	7.63 ± 0.030			
	UV-metric	pK_a	5.62 ± 0.035			
		psK_a	7.66*			
	pH-metric	pK_a	5.19 ± 0.040			
		psK_a	5.80 ± 0.040			
Etoposide	Fast UV	pK_a	9.79 ± 0.021		9.33	9.33
		psK_a	10.10 ± 0.050			
	UV-metric	pK_a	8.66 ± 1.690			
		psK_a	10.13*			
	pH-metric	pK_a	10.19 ± 0.020			
		psK_a	11.12*			
Glimepiride	Fast UV	pK_a	4.78 ± 0.290		5.62	5.63
		psK_a	5.78 ± 0.150			
	UV-metric	pK_a	6.07 ± 0.125			
		psK_a	6.36 ± 0.080			
Lopinavir	Fast UV	pK_a	11.64 ± 0.463		13.98	1.99 3.71 13.39
		psK_a	12.34 ± 0.220			
	UV-metric	pK_a	11.71 ± 0.049			
		psK_a	13.08 ± 0.050			
Losartan	Fast UV	pK_a	3.11 ± 0.051	4.30 ± 0.016	3.85 5.85	3.82 4.26
		psK_a	3.21 ± 0.020	4.33 ± 0.010		
	UV-metric	pK_a	3.07 ± 0.043	4.35 ± 0.020		
		psK_a	3.21*	4.40*		
	pH-metric	pK_a		5.10 ± 0.030		
		psK_a		5.18 ± 0.110		

Nelfinavir	Fast UV	pK_a	7.83 ± 0.330	9.91 ± 0.055	6.41 9.28	2.16 7.01 9.28
		psK_a	6.48 ± 0.040	9.90 ± 0.020		
	UV-metric	pK_a	6.38 ± 0.187	10.48 ± 0.241		
		psK_a	6.40 ± 0.060	10.35 ± 0.000		
	pH-metric	psK_a	4.63 ± 0.280	9.11 ± 0.990		
Nicardipine	Fast UV	pK_a	8.01 ± 0.086		8.10	4.33 8.10
		psK_a	7.42 ± 0.010			
	UV-metric	pK_a	7.56 ± 0.466			
		psK_a	7.35 ± 0.020			
	pH-metric	pK_a	n.e.			
		psK_a	7.47 ± 0.02			
Quinacrine	Fast UV	pK_a	8.03 ± 0.020	10.32 ± 0.065	8.37 10.33	8.02 10.92
		psK_a	8.06 ± 0.040	10.49 ± 0.020		
	UV-metric	pK_a	8.02 ± 0.013	10.29 ± 0.057		
		psK_a	8.12 ± 0.050	10.89 ± 0.140		
	pH-metric	pK_a	8.20 ± 0.050	9.77 ± 0.070		
		psK_a	7.98 ± 0.130	10.21 ± 0.120		
Quinidine	Fast UV	pK_a	4.41 ± 0.017	8.63 ± 0.051	4.42 8.55	4.42 8.55
		psK_a	4.35 ± 0.050	8.84 ± 0.010		
	UV-metric	pK_a	4.45 ± 0.006	8.70 ± 0.016		
		psK_a	4.36 ± 0.040	8.91 ± 0.030		
	pH-metric	pK_a	4.33*	8.67*		
		psK_a	4.15 ± 0.080	8.78 ± 0.040		
Ranitidine	Fast UV	pK_a	2.12 ± 0.006	7.11 ± 0.095	0.47 8.30	0.47 8.30
		psK_a	2.12 ± 0.030	7.42 ± 0.030		
	UV-metric	pK_a	2.16 ± 0.016	7.19 ± 0.035		
		psK_a	2.11 ± 0.060	7.44 ± 0.020		
	pH-metric	pK_a	1.96*	8.46*		
		psK_a	2.56 ± 0.050	8.52 ± 0.040		
Ritonavir	Fast UV	pK_a	2.35 ± 0.045		2.21 2.84	2.16 2.70 3.29
		psK_a	2.34 ± 0.040			
	UV-metric	pK_a	2.32 ± 0.008			
		psK_a	1.92 ± 0.190			
Rhodamine 123	Fast UV	pK_a	3.18 ± 0.046		2.85 5.50	2.88 6.20
		psK_a	n.e.			
	UV-metric	pK_a	3.15 ± 0.004			
		psK_a	3.17**			
	pH-metric	pK_a	3.17 ± 0.010			
		psK_a	n.e.			
Triamcinolone	Fast UV	pK_a	10.30 ± 0.558		11.75	11.75
		psK_a	n.d.			
	UV-metric	pK_a	10.66 ± 0.367			
		psK_a	n.e.			

4.1.1 Measurement interferences and technical considerations

Most of the measurements yielded excellent data, and the software displayed no errors or warnings. Since the data was of high quality, minimal refinement was necessary. The titration curves of Hydrochlorothiazide (HCT) presented in figure 5 exemplify the quality of the data obtained.

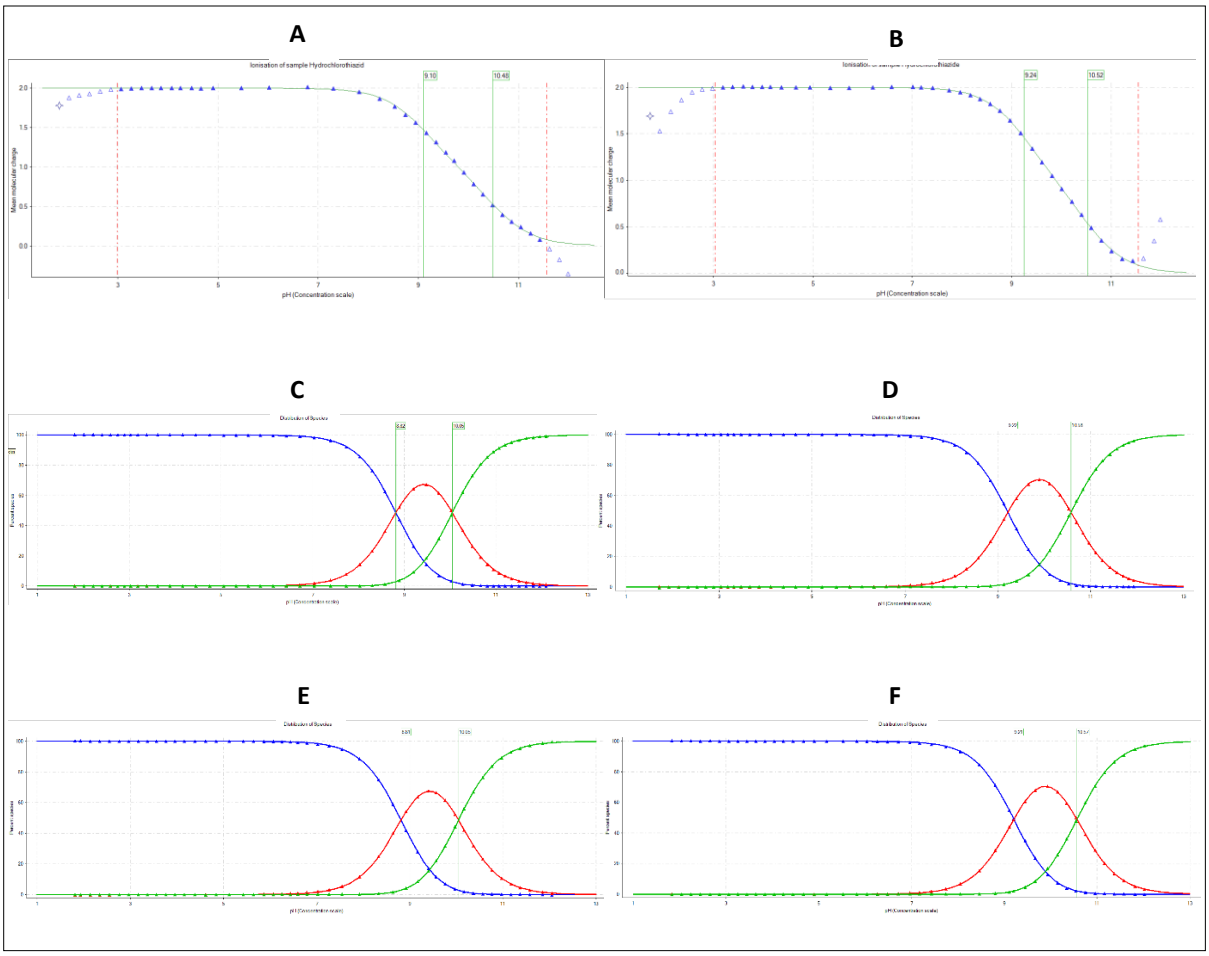

Figure 5: Titration curves for Hydrochlorothiazide. (A) pH-metric pK_a determination. (B) pH metric psK_a determination. (C) Fast UV pK_a determination. (D) Fast UV psK_a determination. (E) UV-metric pK_a determination. (F) UV-metric psK_a determination.

Nevertheless, some of the compounds showed limitations regarding the methods or challenges with turbidity. The measurement of pK_a values using spectrophotometric and potentiometric methods is typically carried out in aqueous solutions, but if compounds have low solubility in water, it is necessary to use a cosolvent such as methanol. In this validation project all compounds were measured with water and cosolvent (methanol/water mix) to assess the performance of the SiriusT3 system.

During the study, individual compounds showed their own unique properties and challenges. One such compound was Candesartan cilexetil. The system and algorithm used for pK_a determination relied on the information provided by the user. When inputting a prediction of three pK_as, the system struggled to identify all three, while reducing the prediction to two pK_as produced clearer titration curves but with inconsistent pK_a values across different methods. However, using a cosolvent in the

measurement resulted in reliable and precise determinations with low standard deviation. Linagliptin only showed one detectable pK_a with pH-metric measurements. This is often the case for compounds with significant UV activity, in which case UV spectroscopy may be the preferred method for pK_a determination. Furthermore, the detected acidic pK_a for Linagliptin laid outside of the detection range.

During the measurement and analysis of (+)-PHNO HCl several problems were encountered. For the Fast UV measurements only one titration was evaluable. The UV-metric measurements however, delivered analysable result. These difficulties could be attributed to the fact, that the measured sample was the salt of (+)-PHNO. The presence of a salt like hydrochloride can potentially change the pK_a that is determined. The salt can affect the ionization state, which in turn can affect the absorbance properties of the sample. The presence of a salt increases the ionic strength of the solution, which can shift the equilibrium between protonated and deprotonated forms. Since the pK_a value is dependent on the equilibrium, this results in a change of the measured pK_a.

During the measurement of psK_a values of some compounds, including Triamcinolone, Rhodamine 123, Etoposide, Atorvastatin, Miconazole and Cetirizine, turbidity problems were encountered when using cosolvent. Titration with water resulted in reliable outcomes, but the utilization of cosolvent led to partially or completely uninterpretable results due to turbidity issues. Possible reasons for the turbidity problems with the cosolvent could be the presence of insoluble compounds, because the addition of the organic solvent can induce precipitation of the compound being measured, especially if it has limited solubility in the solvent mixture. When precipitation occurs, it can lead to the formation of turbidity or cloudiness in the solution, which can interfere with the accurate measurement of the pK_a. Triamcinolone, Etoposide and Cetirizine are soluble in water, therefore in a usual setting, measurements would only be done with water as there is no need for extrapolation afterwards. Rhodamine 123, Atorvastatin and Miconazole on the other hand show a low solubility in water and a titration with methanol/water mixture is recommended. However, the obtained results were not evaluable due to turbidity. It is important to note that highly insoluble compounds may not dissolve in methanol/water mixtures, which is the most commonly used cosolvent on the SiriusT3 instrument. In such cases, other cosolvent systems, such as MDM-mix and dioxane, may be utilized, but pK_a extrapolations from these solvents are valid over a narrower range. As a limitation and future possibility, it is worth noting that the use of MDM mix was not explored in this study. Therefore, it could be used in future studies to evaluate its effectiveness in dissolving highly insoluble compounds and obtaining accurate pK_a values. Additionally, Rhodamine 123, a tautomeric compound (See figure 6) only had one detectable pK_a. One possible explanation could be, that the protonation of one amine affects the electronic distribution and the equilibrium is shifted. The second pK_a might then be outside the detection range (2-12) of the SiriusT3 system. The second possibility is, that the tautomeric forms

may be in rapid equilibrium, making it difficult to distinguish between them experimentally. In this case, the measured pK_a value may represent an average of the two tautomeric forms. Similarly, Ritonavir only showed one pK_a, despite two being predicted. This was likely due to the close proximity of the two pK_as, as they both originate from the amine group in the thiazole rings. Additionally, they are at the edge of the detection range. Bisantrene, a compound that shows structural symmetry (see figure 6), also displays only one detectable pK_a. This symmetry may not only explain the determination of one pK_a, but also the variance between the results obtained from different measurement methods.

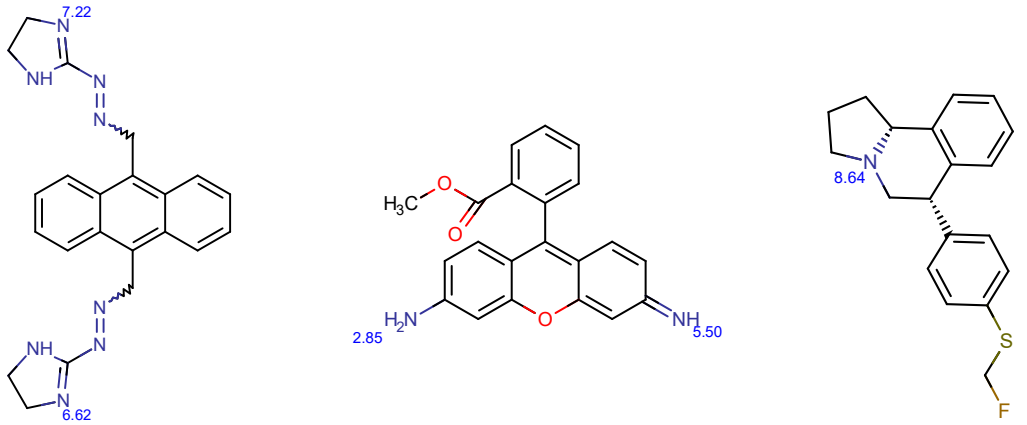

Figure 6: Structure of Bisantrene, Rhodamine 123 and (+)-FMeMcN 5652 (from left to right) and predicted pK_as from MarvinSketch.

Analysis of the data from measuring (+)-FMeMcN 5652 posed difficulties, and results were not reliable. Results displayed great discrepancies between each determination method and even within the same method between individual titrations. (See table 4). When analysing the spectrum obtained through UV-metric method, there was no change in the spectrum. This indicates that the molecule's UV activity was not strong enough to enable UV-metric determination. Because of limitations regarding the sample quantity, measurements could not be repeated with the potentiometric method, even though in this case it would have been the preferred method.

For all pH metric measurements, the sample dissolution method was utilized, which involves stirring the assay medium at a pH where the sample is most soluble for a specified period. However, during the first titration, it was observed that often the results were not evaluable due to turbidity, which could be attributed to insufficient dissolution of the sample. It was noted that during the second titration, the sample dissolved, and the results were evaluable. As a minimum of 25% of the sample curve prior to precipitation is required for determining a pK_a, the first titration could often not be evaluated, resulting in only two evaluable curves and subsequently no standard deviation was calculated for these results.

To address this issue, the titrant pre-dose function could be employed, which dispenses a small volume of titrant from the top of the vial onto the sample. The extreme pH environment created by this function may help to dissolve very weak acids ($pK_a > 11$) or very weak bases ($pK_a < 3$). However, it should be noted that this may cause sample degradation in some cases. Although this method was not employed in this master thesis, it could be considered as a possibility for future work.

Finally, Losartan showed only one pK_a when measured using potentiometry, as the acidic pK_a was near the lower end of the detection range. However, using a cosolvent in combination with UV-metric measurement resulted in two evaluable titrations.

Overall, the investigation of individual compounds highlighted the importance of selecting the most appropriate measurement method based on the specific properties of each compound, as well as adjusting measurement conditions to yield ideal results.

4.1.2 Assessment of the reliability of obtained data

In this study, the accuracy of pK_a measurements using the SiriusT3 instrument was evaluated using three different methods: Fast UV, UV-metric and pH-metric and comparing the obtained results.

Figure 7 is a visual presentation of the mean values of all methods used per compound and the resulting standard deviation. The minimal standard deviations indicate that the instrument delivered precise and accurate results. The data showed minimal variation between the different measurement methods, with the standard deviations under 0.7 for 43 of 46 samples. Two compounds, Bisantrene and Miconazole, showed a SD over 1 and (+)-FMe-McN-5652 yielded a SD over 2. Regarding Bisantrene, the variance is likely due to the symmetry of its structure, as all three measurement methods could only detect one pK_a. During the measurement of Miconazole turbidity problems were encountered when using cosolvent, resulting in bigger variances between the measurements. (+)-FMe-McN-5652 showed great discrepancies, because the spectrophotometric determination was not applicable, as discussed earlier.

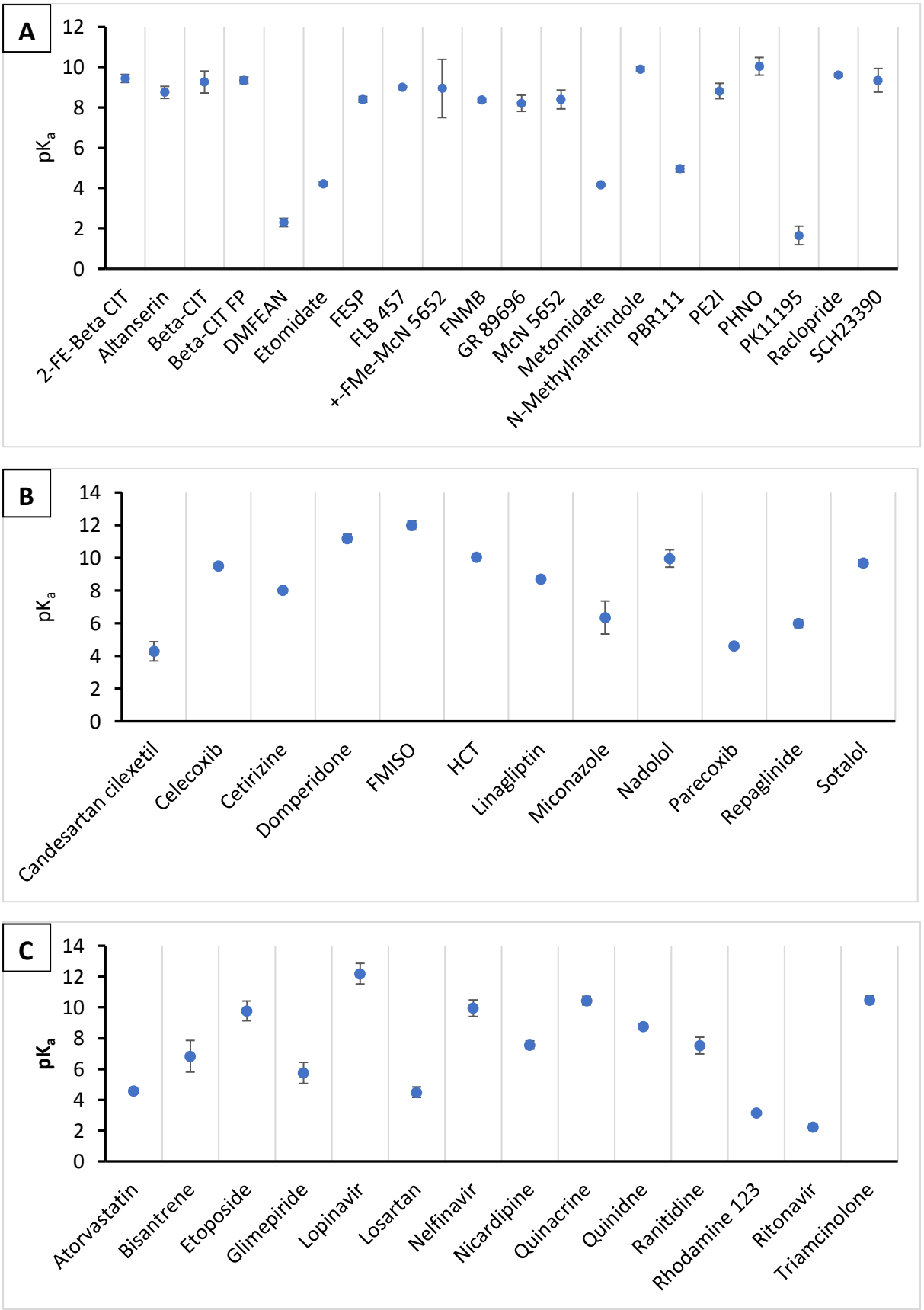

Figure 7: Graphical analysis of measurement accuracy. (A) BBB penetrating compounds, (B) BBB non-penetrating compounds, (C) compounds that interact with efflux transporters. The dots and whiskers represent the mean and SD of all performed measurements. In case where a compound has multiple pK_as, only the most basic pK_a is presented in the graph.

In order to further assess the accuracy of the determined pK_a values, a comparison to literature values was performed. Literature research led to limited results and not all measured compounds had published data available. For PET radiotracers, experimental data was particularly scarce, and most publications relied on calculated values. In table 7, the measured pK_a represents the mean of all measurements performed on each compound. Upon comparison of the obtained experimental data with published values, it was observed that the overall variances were low. However, published data was obtained using different measurement techniques, such as spectrophotometry, potentiometry and NMR. Some of the literature values were not directly measured but are instead an estimation of the ionization constant through means of electrophoresis. This leads to limitations regarding the applicability of direct comparison.

The compounds that showed significant differences from the experimental data were Celecoxib, Glimepiride, HCT, Nicardipine, Rhodamine 123 and Triamcinolone. Among these, the data obtained for Celecoxib, Glimepiride, HCT and Nicardipine was of excellent quality and highly reliable. The differences observed to literature values could potentially be attributed to differences in measurement methods. However, Rhodamine 123 and Triamcinolone posed challenges during measurement and analysis, which explains the greater variances when compared to published data.

Table 7: Comparison with literature values. Table displays compounds with published experimental pK_a values and the difference to the mean of measured pK_a values.

compound	literature values	measured pK_a	difference
Candesartan cilexetil	4.45 (35)	4.28 ± 0.590	0.17
Celecoxib	11.10 (36)	9.51 ± 0.141	1.59
Cetirizine	2.92; 8.27 (37)	2.65 ± 0.337; 8.00 ± 0.046	0.27; 0.27
Domperidone	11.60(38)	11.19 ± 0.245	0.41
Etomidate	4.20 (39)	4.22 ± 0.080	0.02
Etoposide	9.80 (40)	9.77 ± 0.642	0.03
Glimepiride	7.26 (41)	5.75 ± 0.687	1.51
HCT	7.00; 9.20 (42)	8.81 ± 0.069; 10.04 ± 0.089	1.81; 0.84
Linagliptin	8.60 (43)	8.69 ± 0.063	0.09
Losartan	4.70 (35)	4.50 ± 0.340	0.20
McN 5652	8.52 (44)	8.37 ± 0.465	0.15
Miconazole	6.70 (45)	6.35 ± 1.010	0.35
Nadolol	9.77 (46)	9.97 ± 0.531	0.20
Nicardipine	8.60 (47)	7.56 ± 0.262	1.04
Quinacrine	7.43 (48)	8.07 ± 0.271	0.64
Quinidine	4.00; 8.54 (49)	4.34 ± 0.104; 8.77 ± 0.111	0.34; 0.23
Raclopride	8.97 (50)	9.61 ± 0.073	0.64
Ranitidine	8.31 (51)	7.52 ± 0.542	0.79
Repaglinide	3.83 (46)	4.55 ± 0.242	0.72
Rhodamine 123	7.20 (52)	3.17 ± 0.015	4.03
Sotalol	8.11; 9.65 (53)	8.33 ± 0.124; 9.69 ± 0.207	0.22; 0.04
Triamcinolone	6.15 (54)	10.48 ± 0.255	4.33

Overall, the supportive data shows that the accuracy of the measurements is very high, and the determination of the ionization constant with the SiriusT3 delivers accurate, reliable and reproducible results. The minimal variation between the different measurement methods indicate that the instrument delivers consistent results, making it a useful tool in drug discovery. However, it is important to note that there is no comparison to other measurement methods such as NMR spectroscopy and literature values were not available for all compounds. These limitations suggest that further studies may be needed to fully validate the accuracy of the SiriusT3 instrument, especially for compounds with complex structure, low solubility or weak UV-activity.

4.2 Assessment of importance of experimental pK_a determination

The aim of this study was to evaluate whether calculated pK_as are reliable, or if an experimental determination is necessary. The pK_a value is a significant physicochemical parameter in drug discovery due to its relevance for the pharmacokinetic properties of drugs. Hence, having precise and reliable pK_a values is of utmost importance. The results obtained clearly demonstrate that there is a considerable discrepancy between the measured and calculated values, suggesting that if one desires an accurate value, it is essential to measure it.

To visualize the deviation between the measured and calculated pK_a values, a bar chart was created, which illustrates the deviation of the measured pK_a values from the calculated ones (See figure 10). The chart displays considerable variances between compounds and that 15 out of 46 compounds exhibit a deviation greater than 1, indicating a significant difference between the measured and calculated values.

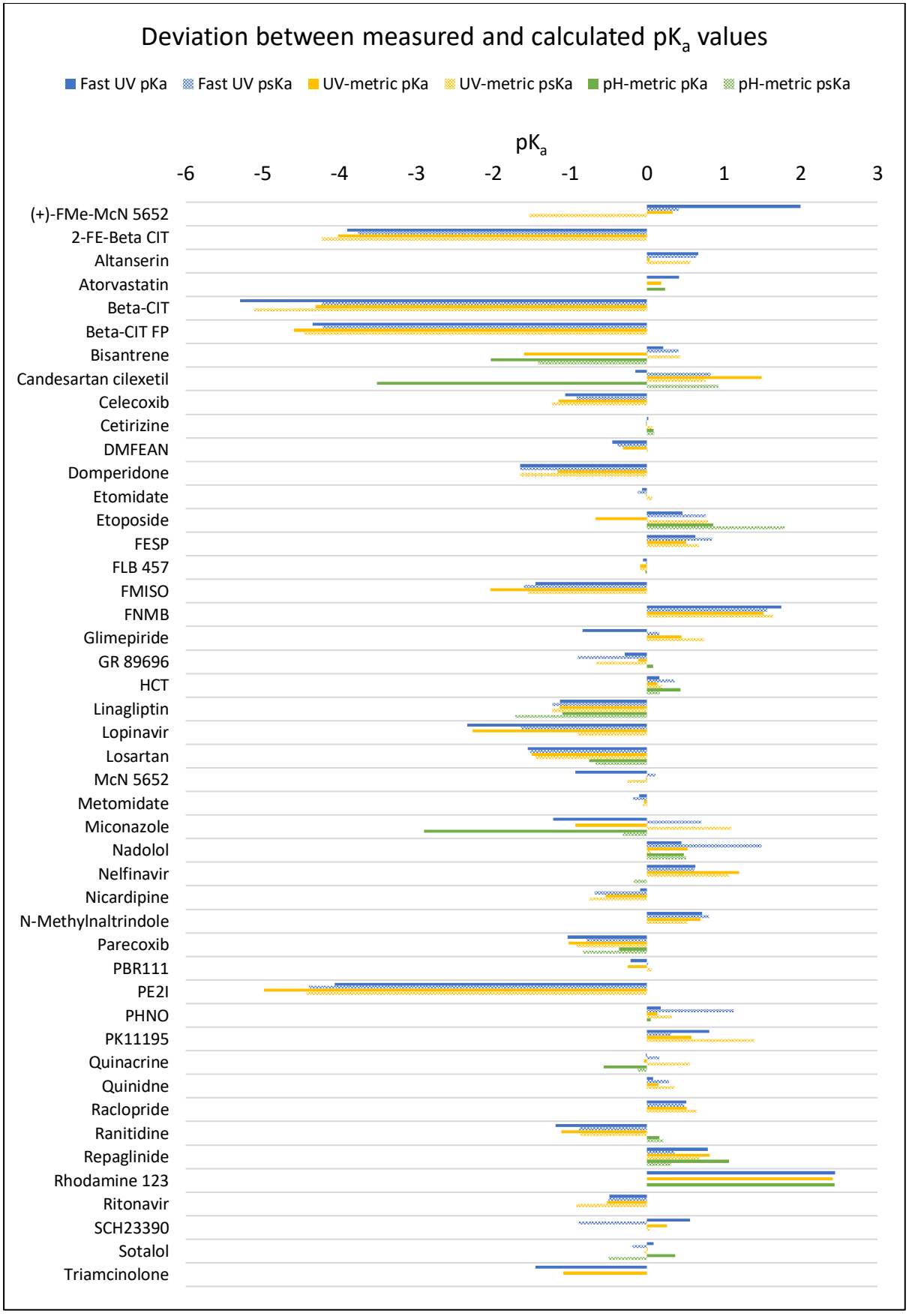

Figure 8: Deviation of the measured pK_a from the calculated values for all 46 analysed compounds. The bars represent the deviation of the pK_a values towards the acidic or basic side. In case where a compound has multiple pK_as, only the most basic pK_a is presented in the graph.

Furthermore, it was observed that occasionally MarvinSketch and Chemicalize predict different pK_a values. The two programs are based on different algorithms and databases, which can result in variations, particularly for certain functional groups. When analysing the data, it became apparent that these discrepancies occurred specifically with the carbonyl group of an amide. This observation involved FESP, GR-89696, PBR 111, PK 11195, Lopinavir, Nelfinavir, Ritonavir and Repaglinide. MarvinSketch predicted pK_a values for the carbonyl group, whereas Chemicalize did not. When compared to the measurements, the carbonyl group did not lead to a detectable pK_a. Exemplarily the structure of FESP is shown in figure 11. According to the structure of the compound, theoretically the carbonyl group could protonate but in reality, it would only do so in highly acidic solutions and even then, it is very unlikely. This explains why only one pK_a is detected. Chemicalize considers empirical data, which can explain the exclusion of the carbonyl group from the prediction, thus prediction with Chemicalize was more accurate. In an analogous manner, GR-89696 shows differences in the pK_a prediction. In addition to the above explanation, the presence of fumarate can potentially change the pK_a that is determined.

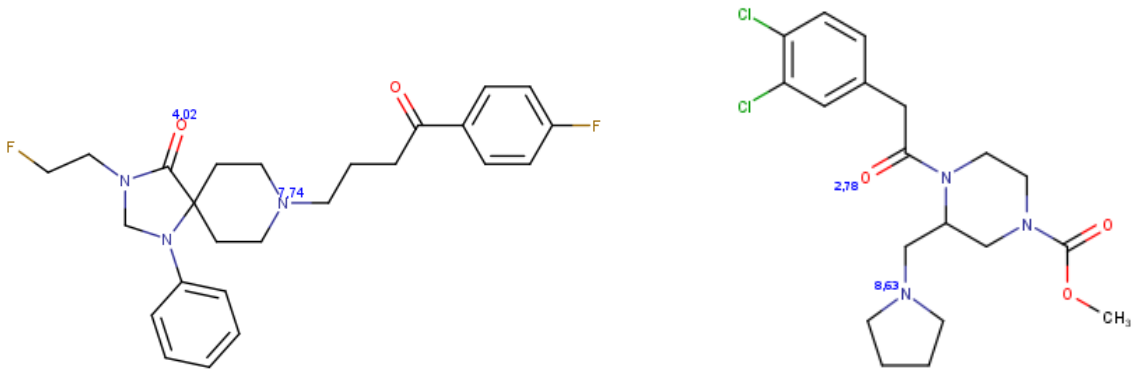

Figure 9: Structure of FESP and GR-89696 and predicted pK_as from MarvinSketch.

Mostly, the predictions are either the same, or variances are minor. Compounds, where the calculations highly differ are 2-FE-Beta-CIT, Beta-CIT, Beta-CIT-FP and PEI2. The structural properties of these compounds are very similar, as they are all derivates of Tropane (See figure 12). In these instances, when compared to the experimental data, the calculations from MarvinSketch are more accurate.

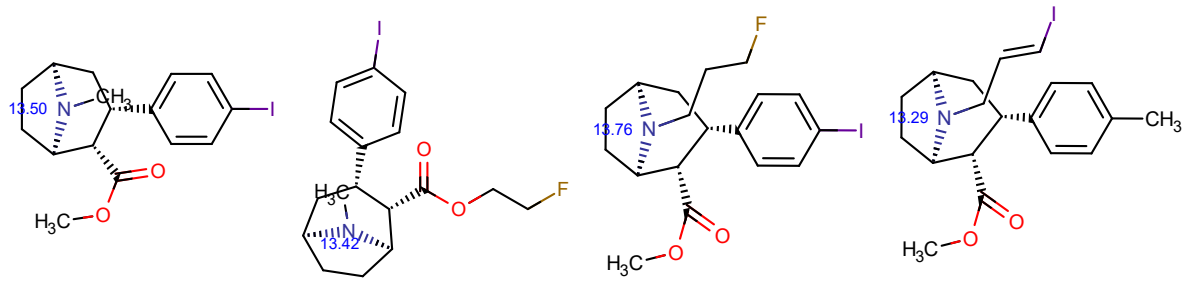

Figure 10: Structures of Beta-CIT, 2-FE-Beta-CIT, Beta-CIT-FP, PE2I (from left to right).

Settimo et al. report a difference in prediction accuracy between acids and bases. (55) To see if this difference can be observed within this set of compounds, the samples were divided into acids and bases. Figures 13 and 14 graphically show the deviation in a bar chart. 25% of the acids and 33% of the bases displayed deviations greater than 1. When considering, that MarvinSketch delivered more accurate predictions for 2-FE-Beta-CIT, Beta-CIT, Beta-CIT-FP and PE2I, the percentage of deviation for the set of bases, reduced to 20%. Subsequently, there was no considerable difference in accuracy between acids and bases. However, this set of compounds consists of drugs and diagnostic agents, consequently all the substances are weak bases or weak acids, which can possibly affect these findings.

It is important to note, that pK_a prediction is a complex task and different methods may be more accurate for certain types of compounds or functional groups. The findings of this study provide valuable information regarding the necessity of comparison of multiple methods and experimental data. Measuring pK_a values instead of solely relying on calculated values is inevitable and could help in better drug design and optimization by providing more accurate parameters for pharmacokinetic studies. In conclusion, the study suggests that calculated pK_a values should be taken with caution and that the measurement of pK_a values is a crucial step in drug discovery.

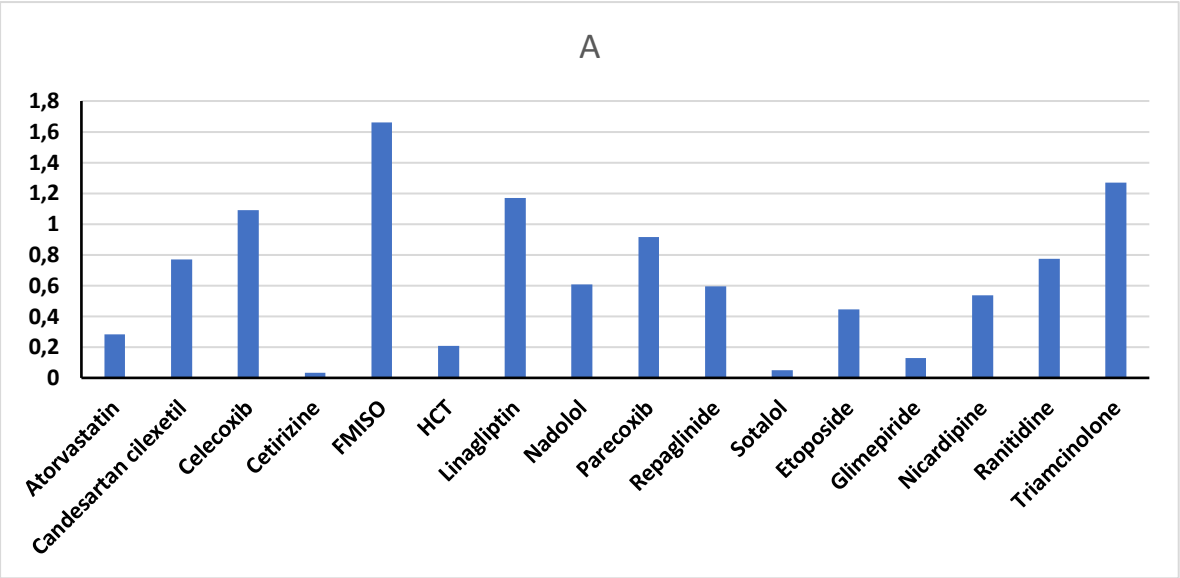

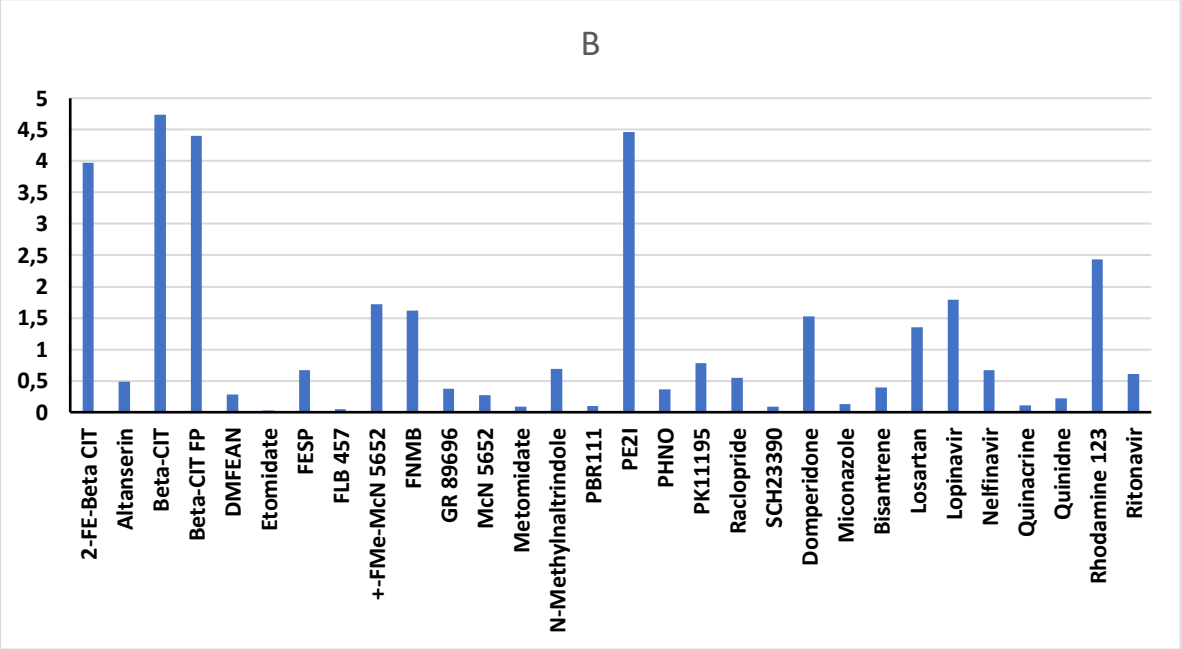

Figure 11: Deviation of predicted pK_a values from experimental data for (A) a set of acids and (B) a set of bases.

4.3 Review CNS MPO score

Generally, a compound with a CNS MPO score of 3 or higher is considered to have the potential for CNS activity. However, it is important to note that the CNS MPO score is just one of many factors that are considered when assessing a compound's potential for CNS activity. Data accumulated within this master thesis suggest that the CNS MPO score should not be used in isolation and should be considered alongside other factors.

During this project a total of 20 compounds that were known to be BBB penetrating were analysed and their CNS MPO score was determined (See table 8).

Table 8: CNS MPO score for CNS active compounds and their respective experimental pK_a value (mean of all performed measurements of each compound). In case a compound has more than one pK_a, only the most basic is presented in the table.

Compound	pK_a	CNS MPO score
2-FE-Beta CIT	9.44 ± 0.199	4.06
Altanserin	8.75 ± 0.298	4.46
Beta-CIT	9.27 ± 0.543	4.35
Beta-CIT FP	9.36 ± 0.158	3.76
DMFEAN	2.30 ± 0.203	4.73
Etomidate	4.22 ± 0.080	5.75
FESP	8.41 ± 0.141	4.68
FLB 457	9.02 ± 0.038	5.13
(+)-FMe-McN 5652	6.92 ± 2.095	3.30
FNMB	8.37 ± 0.100	5.37
GR-89696 fumarate	8.21 ± 0.400	5.29
McN 5652	8.40 ± 0.465	3.23
Metomidate	4.16 ± 0.064	5.93
N-Methylnaltrindole	9.91 ± 0.117	4.47
PBR111	4.96 ± 0.158	4.68
PE2I	8.82 ± 0.381	3.49
(+)-PHNO HCl	10.05 ± 0.439	5.04
PK11195	1.66 ± 0.461	3.66
Raclopride	9.61 ± 0.073	4.97
(-)-SCH23390 HCl	9.35 ± 0.586	3.66

The results showed that all the BBB penetrating compounds yielded scores above the threshold of 3, suggesting that the CNS MPO score may be a useful tool for predicting the potential for CNS activity. However, caution should be taken when using the CNS MPO score as a sole predictor of CNS activity, as it was observed that 8 out of 12 analysed compounds that were known to be BBB non-penetrating had scores over 3 as well (See table 9). This observation suggests that a high CNS MPO score is not always a reliable predictor of CNS activity and BBB penetration, and additional testing and analysis is required to fully evaluate a compound's pharmacological properties. Despite this, it is important to note that compounds with scores lower than 3 are unlikely to be successful candidates for CNS drugs.

Table 9: CNS MPO score for CNS inactive compounds and their respective experimental pK_a value (mean of all performed measurements of each compound).

Compound	pK_a	CNS MPO score
Candesartan cilexetil	4.28 ± 0.590	1.75
Celecoxib	9.51 ± 0.141	3.84
Cetirizine	8.00 ± 0.046	5.54
Domperidone	11.19 ± 0.245	4.92
FMISO	11.98 ± 0.261	5.75
HCT	10.04 ± 0.089	4.05
Linagliptin	8.69 ± 0.063	2.98
Miconazole	6.35 ± 1.010	2.95
Nadolol	9.97 ± 0.531	4.32
Parecoxib	4.62 ± 0.109	5.11
Repaglinide	5.98 ± 0.242	4.65
Sotalol	9.69 ± 0.207	4.43

The CNS MPO score defines pK_a values over 10 as less desirable. Of the 20 BBB penetrating compounds that were analysed, (+)-PHNO HCl has a pK_a over 10. In this study, the salt of (+)-PHNO was measured, which possibly alters the detected pK_a. The CNS MPO score considers six parameters and is therefore more holistic than traditional approaches that rely on strict cut-offs for individual physicochemical parameters. As a result, compounds that have a pK_a over 10, and would fall through in early drug discovery using traditional cut-offs. The CNS MPO score can be used to identify a potential for CNS activity. This highlights the benefits of adopting a more comprehensive approach in drug discovery to identify CNS activity.

Some of these pK_a values suggest that the compounds may be charged at physiological pH of 7.4. This would prevent passive diffusion across the BBB or at least decrease bioavailability. For example, DMFEAN is a very weak base with a pK_a of 2.3, which suggests that it will be fully protonated at physiological pH and will have a positive charge. There is currently no information whether it is transported actively across the BBB. Luurtsema et al. report the uptake of metabolites of DMFEAN. (56) Given the charge at physiological pH, passive diffusion is unlikely, and a transporter-mediated mechanism is possibly involved. Similarly, PK11195 has a pK_a of 1.6, which also indicates that it will be fully protonated and positively charged at pH 7.4. PK11195 is known to use the peripheral benzodiazepine receptor (PBR) as a transporter to cross the BBB. (57) Etomidate and Metomidate can penetrate the BBB, despite their pK_a values of 4. These compounds are both small, lipophilic and have a low molecular weight. At physiological pH they will be partially ionized, but the neutral fraction can penetrate the BBB. (58)Similarly, PBR 111 has a relatively low molecular weight and is lipophilic, which

means it can partially cross the BBB by passive diffusion, despite a pK_a of 4.96. However, it is known as a PBR ligand, resulting in active transport. (59)

Another actively transported compound is (+)-FMeMcN5652, a selective ligand for the serotonin transporter (SERT), which is expressed on the endothelial cells of the BBB. (60)Beta-CIT-FP, 2-FE-Beta-CIT and PE2I, all derivatives of beta-CIT, have been shown to bind to the dopamine transporter (DAT) with high affinity and they are commonly used as radioligands for in vivo imaging of the DAT in the brain. (61–63)

On the other hand there are CNS inactive drugs that actually display favourable pK_a values for passive diffusion across the BBB. For example Domperidone is known as a dopamine antagonist to treat gastrointestinal disorders. Interestingly it is structurally similar to other dopamine antagonists like metoclopramide, which is able to cross the BBB, yet Domperidone is not CNS active. A possible explanation could be that Domperidone has a low affinity to dopamine receptors in the CNS, which would classify it as CNS inactive. Even if this substance is able to partially cross the BBB, it may not do so at sufficient levels to produce pharmacological effects. (64)The ionization state may theoretically allow it to penetrate the BBB, but other factors limit the ability to produce CNS effects. Similarly, Nadolol and Sotalol, both beta blockers that act on the cardiovascular system, have the potential to penetrate the BBB and be CNS active according to their pK_a and CNS MPO score. But in fact, both are highly bound to plasma proteins, which greatly limits their ability to diffuse into brain tissue. Furthermore, they are compounds with low lipophilicity and even though beta-adrenergic receptors are present in the CNS, the affinity for these receptors is low. (65,66)

In conclusion the CNS MPO score can be a useful tool in screening for compounds that have the potential for CNS activity. However, it should not be used in isolation and should rather be considered alongside other factors such as in vitro and in vivo testing, pharmacokinetics and safety profiles when assessing a compound’s potential for CNS activity.

5 Conclusion

In conclusion, the evaluation of a fully automated system for pK_a determination was performed by measuring 46 compounds using both spectrophotometric and potentiometric methods. The results demonstrate that the fully automated SiriusT3 instrument generates accurate and reliable data, making it a convenient tool for the determination of physicochemical parameters such as the ionization constant. The instrument allows for rapid measurement of pK_a values in just 6 minutes with minimal sample quantities and preparation.

Additionally, during this master thesis a SOP was developed to provide a comprehensive manual for the determination of the ionization constant using the SiriusT3 instrument and software.

This study highlights the importance of accurate determination of physicochemical parameters, especially the ionization constant, in the drug discovery and development process. The results suggest that implementing the CNS MPO score is a reasonable approach to screen for CNS activity potential, however it solely considers passive diffusion.

Furthermore, the literature search for published experimental data on the pK_a values of the 46 measured compounds was largely unsuccessful, with data available for only a few of the compounds. Despite the inclusion of various physicochemical parameters on sites such as PubChem, it is worth noting that pK_a values are often not displayed for compounds on these platforms. Therefore, this data may be of interest for publication, providing a library of pK_a values and supporting the work of scientists and researchers in the field.

Table of figures

Table of tables

Table of equations

Abbreviations

ACD	acid dissociation calculator
ADME	absorption, distribution, metabolism, excretion
BBB	blood-brain barrier
BCS	biopharmaceutical classification system
BHS	Blut-Hirn-Schranke
CADD	computer-aided drug design
CAS	chemical abstracts service
CNS	central nervous system
CNS MPO	central nervous system multiparameter optimization
DAT	dopamine transporter
EC	endothelial cell
GCP	good clinical practices
GLP	good laboratory practices
GMP	good manufacturing practices
HBD	hydrogen bond donor
HCl	hydrochloric acid
ISA	ionic strength adjuster
IUPAC	International Union of Pure and Applied Chemistry
Ka	acid dissociation constant
KCl	potassium chloride
KHP	potassium hydrogen phthalate
KOH	potassium hydroxide
logD	distribution coefficient
logP	partition coefficient
M	molar
MeOH	methanol
MW	molecular weight
n.d.	not defined
n.e.	not evaluable
NMR	nuclear magnetic resonance
PD	pharmacodynamic
PET	positron emission tomography
PK	pharmacokinetic
pK_a	ionization constant
pK_s	Säurekonstante
psK_a	ionization constant in cosolvent mixture
QSAR	quantitative structure-activity relationship
Ro5	rule of five
SD	standard deviation
SERT	serotonin transporter
SOP	standard operating procedure
TFA	target factor analysis

tPSA	topological polar surface area
UV	ultraviolet
ZNS	zentrales Nervensystem

Appendix

Compound	Structure	MW (g/mol)	CNS MPO score	CNS activity
2-FE-Beta-CIT	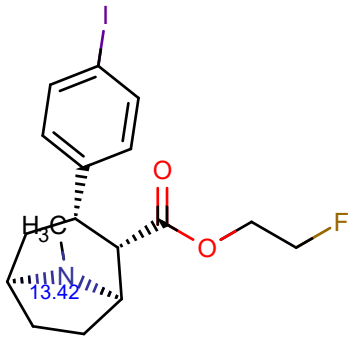	417.26	4.06	+
Altanserin	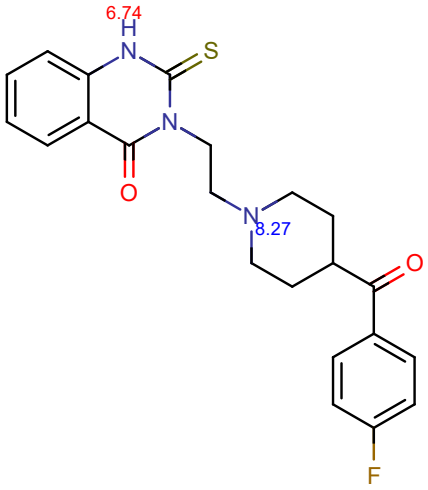	411.50	4.46	+

Atorvastatin	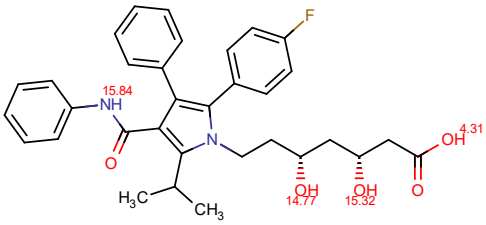	558.65	2.06	x
Beta-CIT	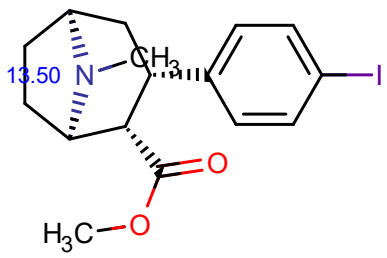	385.25	4.35	+
Beta-CIT-FP	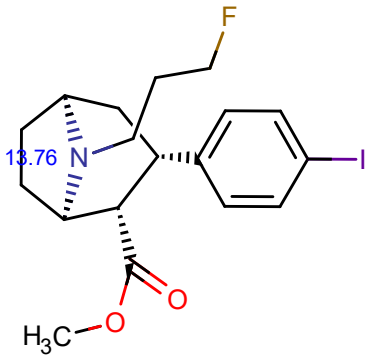	431.29	3.76	+

Bisantrene	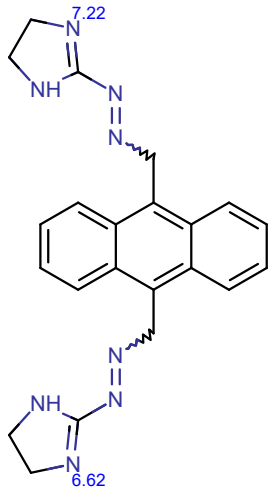	398.47	4.19	x
Candesartan cilexetil	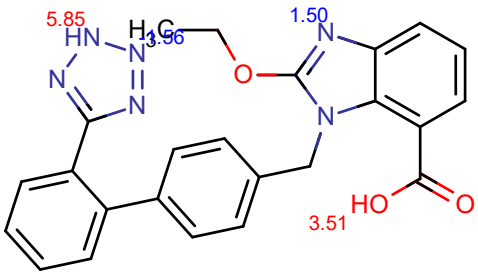	610.67	1.75	-
Celecoxib	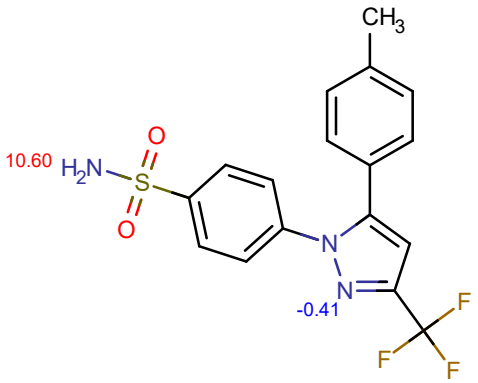	381.37	3.84	-

Cetirizine	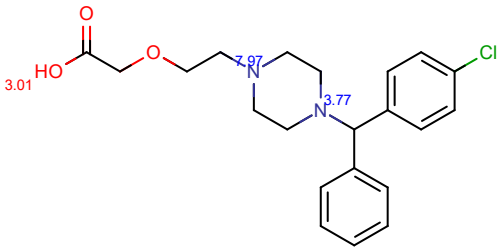	388.89	5.54	-
DMFEAN	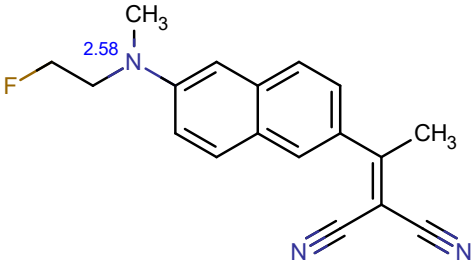	293.35	4.73	+
Domperidone	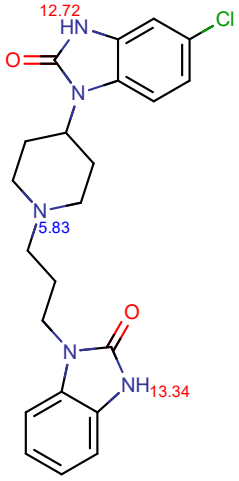	425.92	4.92	-

Etomidate	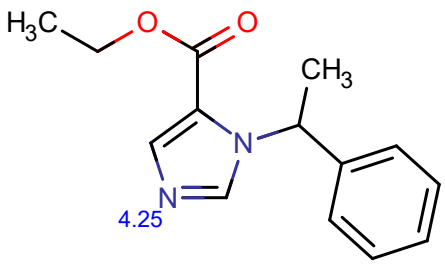	244.29	5.75	+
Etoposide	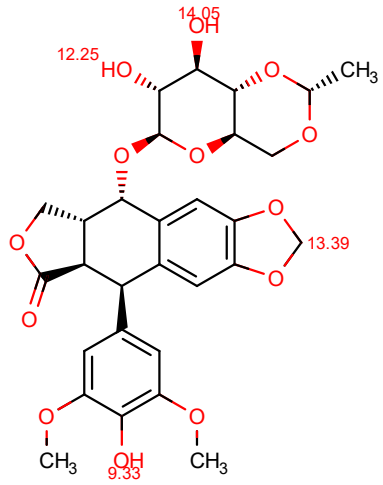	588.56	3.25	x
FESP	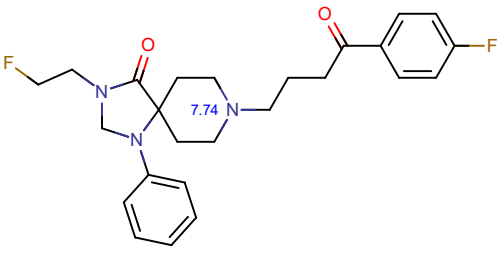	441.52	4.68	+

FLB 457	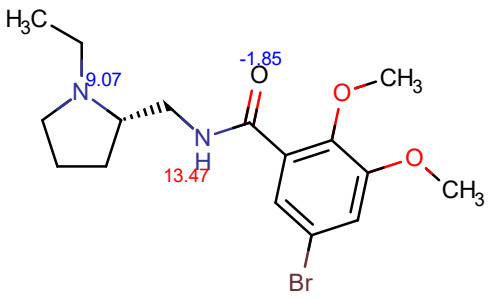	371.27	5.13	+
(+)-FMe-McN 5652	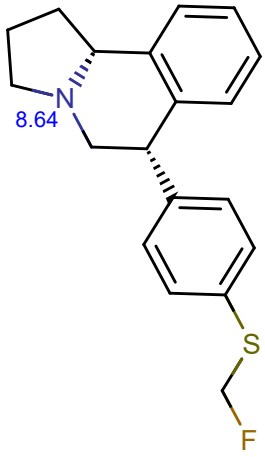	313.43	3.30	+
FMISO	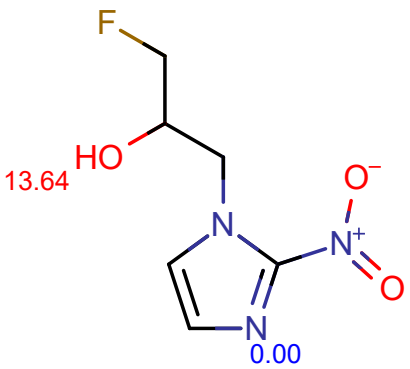	189.15	5.75	-

FNMB	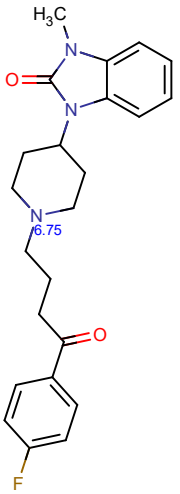	395.48	5.37	+
Glimepiride	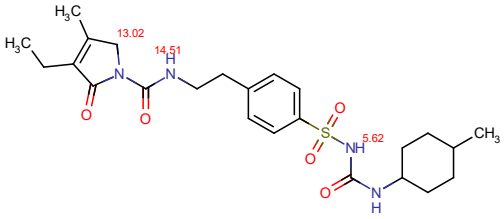	490.62	3.14	-
GR-89696 fumarate	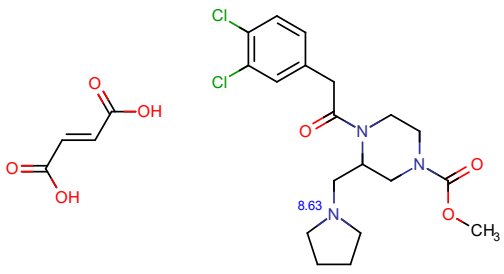	414.33	5.29	+

Hydrochlorothiazide	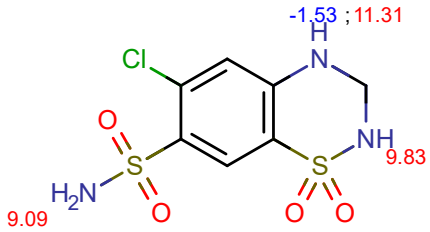	297.73	4.05	-
Linagliptin	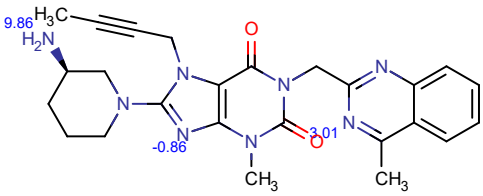	472.55	2.98	-
Lopinavir	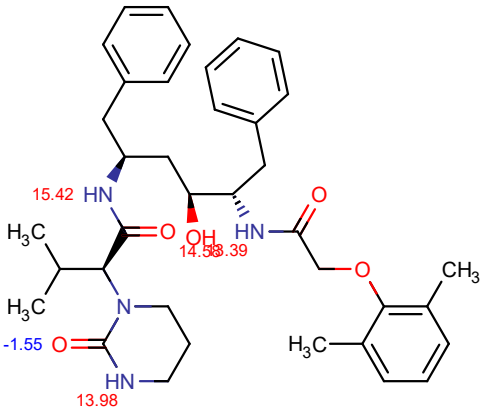	628.81	1.16	x

Losartan	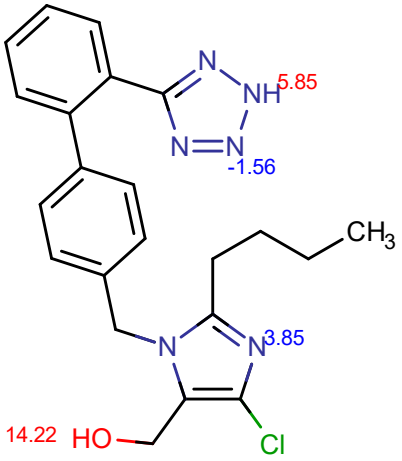	422.92	3.06	x
(+)-McN-5652	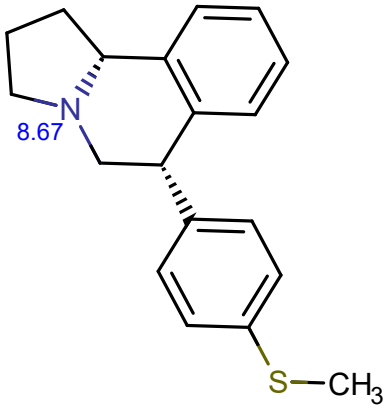	295.44	3.23	+
Metomidate	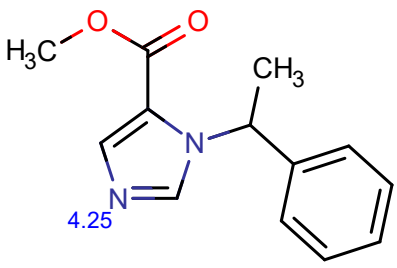	230.27	5.93	+

Miconazole	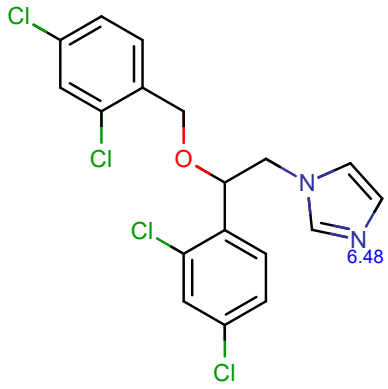	416.12	2.95	-
Nadolol	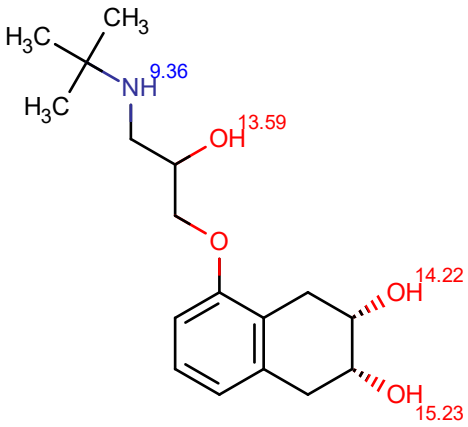	309.41	4.32	-
Nelfinavir	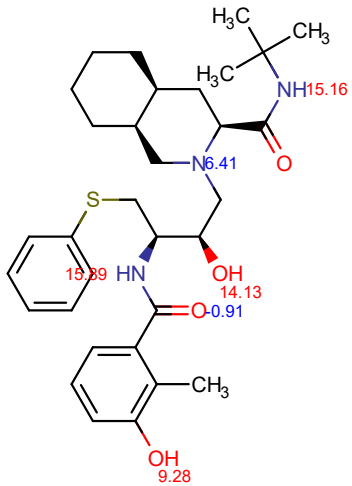	567.79	1.62	x

Nicardipine	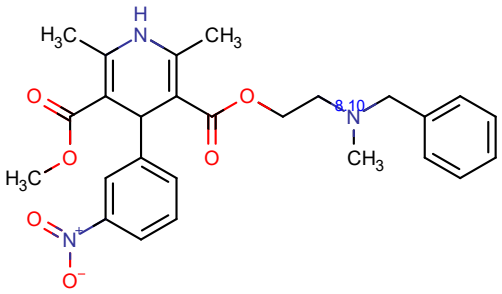	479.53	3.48	x
N-Methylnaltrindole	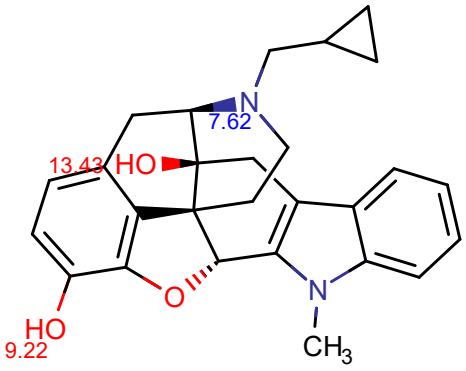	428.53	4.47	+
Parecoxib	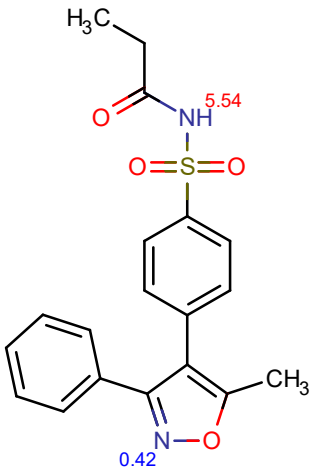	370.42	5.11	-

PBR 111	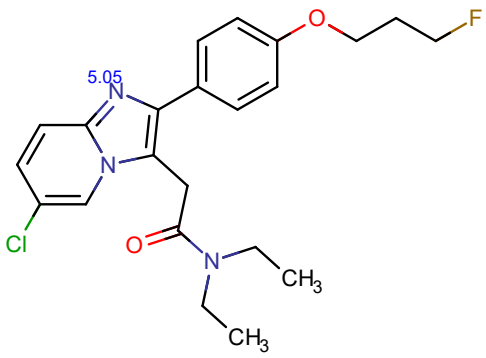	417.91	4.68	+
PE2I	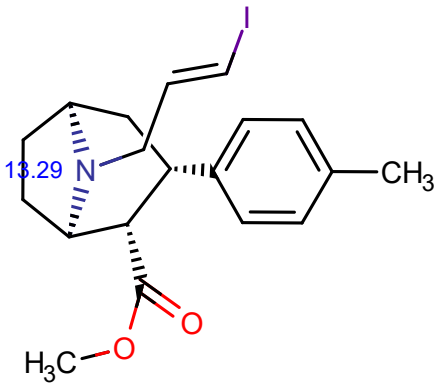	425.31	3.49	+
(+)-PHNO	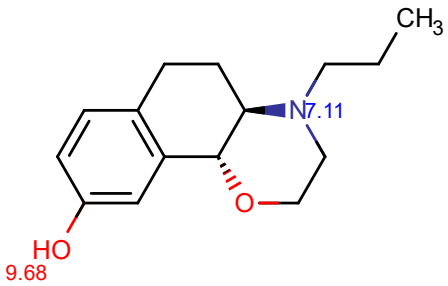	247.34	5.04	+

PK 11195	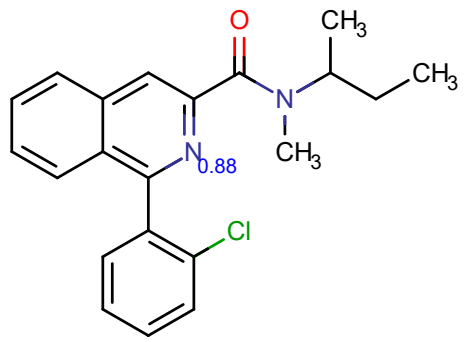	352.86	3.66	+
Quinacrine	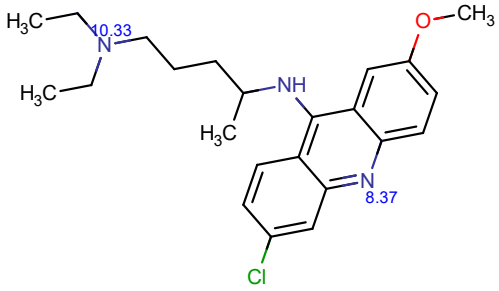	399.96	3.33	x
Quinidine	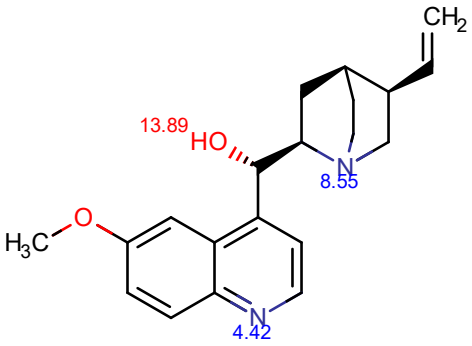	324.42	5.48	x

Raclopride	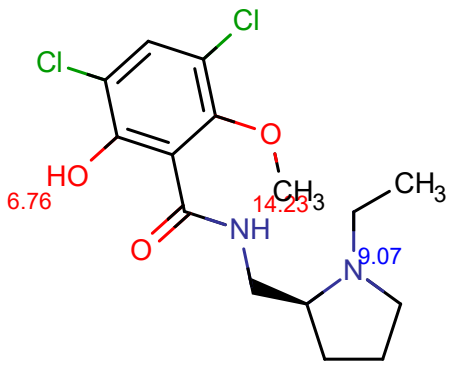	347.24	4.97	+
Ranitidine	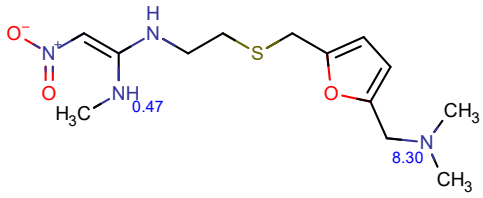	314.40	5.35	x
Repaglinide	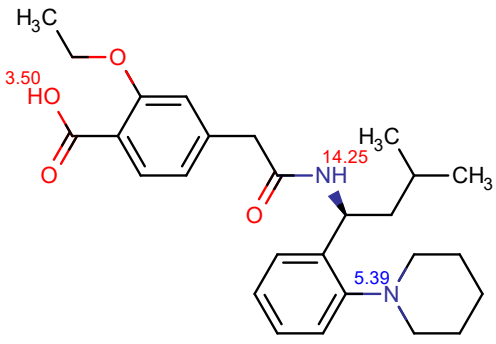	452.60	4.65	-

Rhodamine 123	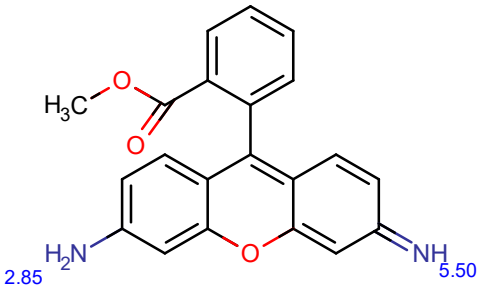	358.40	4.96	x
Ritonavir	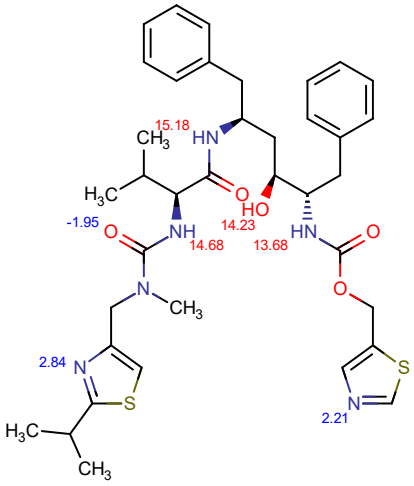	720.95	1.00	x
(-)-SCH23390	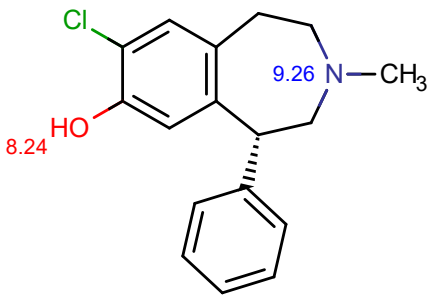	287.79	3.66	+

Sotalol	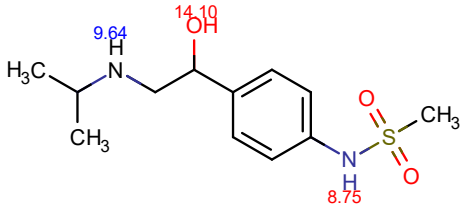	272.36	4.43	-
Triamcinolone	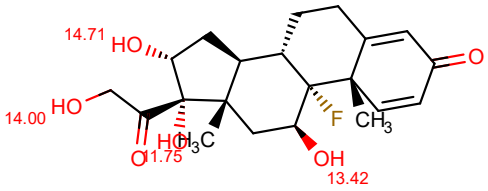	394.44	3.92	x

Measurement of the ionisation constant with SiriusT3

1. APPLICATION AREA

This SOP is valid at the Department of Pharmaceutical Sciences at the Division of Pharmaceutical Chemistry of the University of Vienna. The SOP describes the process of measuring pK_a values with the SiriusT3 instrument.

2. RELATED DOCUMENTS

N.D.

3. RESPONSIBILITIES

N.D.

4. ABBREVIATIONS

ISA	ionic strength adjuster
KCl	potassium chloride
KHP	potassium hydrogen phthalate
KOH	potassium hydroxide
HCl	hydrochloric acid
MeOH	methanol
N.D.	not defined
psK_a	pK_a in cosolvent mixture
SD	standard deviation
SOP	standard operating procedure
UV	ultraviolet

5. REQUIRED MATERIAL

- SiriusT3 instrument including Dispenser module, Titrator module and Autoloader module.
- SiriusT3Control and SiriusT3Refine software
- Potassium chloride (CAS: 7447-40-7, Sigma Aldrich)
- Potassium hydroxide ampoule (Tritisol®, CAS: 1310-58-3, Sigma Aldrich)
- Potassium hydrogen phthalate (≥99.95%, CAS: 877-24-7, Sigma Aldrich)
- Methanol (≥99.9%, CAS: 67-56-1, Sigma Aldrich)
- Anhydrous di-potassium hydrogen orthophosphate (CAS: 7785-11-4, Sigma Aldrich)
- Hydrochloric acid (≥37%, CAS: 7647-01-0, Sigma Aldrich)
- Fast UV buffer (Pion Inc. T1404007)
- pH 7.00 buffer solution (Certipur®, Sigma Aldrich)
- Triton® X-100 (CAS: 9036-19-5, Sigma Aldrich)
- 2-propanol (≥99.8%, CAS: 67-63-0, Sigma Aldrich)
- Purified water

6. PROCEDURE

Preparatory steps:

- Preparing the reagents for the measurements:
    - 1 L of Ionic-Strength Adjusted Water (0.15 M KCl):
        - Label a 1 L volumetric flask with “ISA water 0.15 M KCl” and date.
        - Weigh out 11.18 g ± 0.1 g KCl.
        - Transfer the weighed KCl to a volumetric flask.
        - Make up to the 1 L mark with purified water, seal and invert flask several times until solution is fully mixed.
        - Transfer the contents of the volumetric flask to the respective plastic reagent bottle.
    - 1 L of Base (0.5 M KOH):
        - Label a 1 L volumetric flask with “Base 0.5 M KOH” and date.
        - Place a KOH ampoule into the volumetric flask and firmly pierce the seals, following the instructions supplied.
        - Rinse ampoule three times with purified water.
        - Make up to the 1 L mark with purified water.

        - Transfer the contents of the volumetric flask to the respective plastic reagent bottle.
        - When changing the KOH on the instrument, the KHP standardization procedure must be carried out.
    - 1 L of Ionic-Strength Adjusted Methanol (80% methanol, 20% ISA water):
        - Label a 1 L volumetric flask with “80% Methanol + 20% ISA water” and date.
        - Add 200 mL of purified water to the flask.
        - Make up almost to the mark with methanol and shake well to mix.
        - Methanol will degas when mixed with water, so leave to settle and come to room temperature before accurately making up to the 1 L mark with methanol.
        - Transfer the contents of the volumetric flask to the respective plastic reagent bottle.
    - Phosphate Buffer for UV-metric pK_a Analysis:
        - Label a suitable size bottle with “Phosphate Buffer” and date.
        - Weigh out 0.50 g ± 0.02 g of di-potassium hydrogen orthophosphate.
        - Transfer the weighed phosphate to a 200 mL measuring cylinder.
        - Make up the volume to 200 mL with ISA water.
    - 1 L of Acid titrant (0.5 M HCl):
        - Label a 1 L volumetric flask with “Acid titrant 0.5 M HCl” and date.
        - Add 49 mL HCl to the volumetric flask.
        - Make up to the 1 L mark with purified water.
        - Transfer the contents of the volumetric flask to the respective plastic reagent bottle.
- Fill the neutral linear buffer (Fast UV buffer) in the respective plastic reagent bottle.
- Refill the flowing wash water container and empty the flowing wash waste container.

Routine Maintenance Procedure:

- Daily Tasks:
  - Flush the syringes.
    - Click **Flush** in the Dispenser view.
    - In the pop-up window select the dispensers and the corresponding volume to be flushed.
    - Click **OK.**
    - This is performed automatically every morning at 08:00 if there is power to the instrument.
  - Refresh all solutions on the Sample Stage.

    - Select component highlighted in yellow.
    - Click Refresh and enter the current date in the pop-up window.
    - Refill the vial with correct solution.
    - When refilling the storage solution with purified water double click **Waiting for user to refresh** once the vial is refilled with fresh water.
    - Repeat until all components highlighted in yellow have been refreshed.
  - Calibrate the spectrometer.
    - Go to the Spectrometer view, click **Lamp On** and wait 15 minutes until the lamp is warmed up and stabilised.
    - After the lamp settle time is over, click **Calibrate** and select Flowing wash as Location in the pop-up window.
    - Check that the spectrometer integration time is set appropriately, and the max peak intensity falls within the green band on the graph (spectrum will change from red to green at an acceptable intensity).

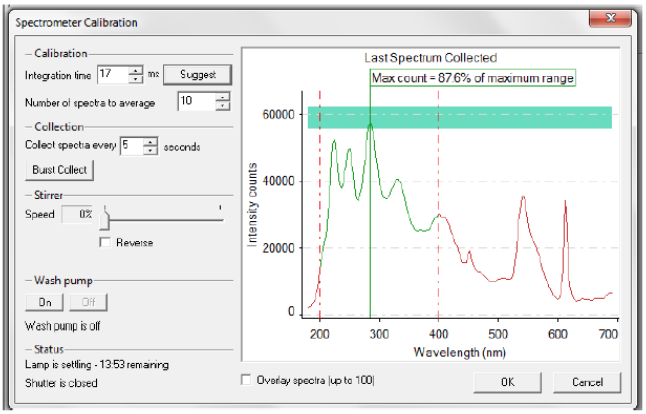

- Refill pH electrode.
    - Go to the pH electrode view and click **Refill.**
    - Refill the pH electrode with KCl filling solution.
    - Finish by clicking **OK**.
- Calibrate the system
    - Place three clean vials in the first three positions on the tray.
    - Double click the corresponding position in the autoloader scheduler to create a new assay.
    - Select **Utility** as the Category and **Clean Up** as the Type.

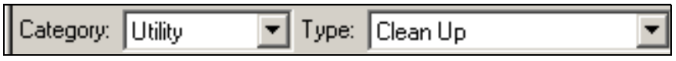

    - Select the titration direction (first assay high to low, second low to high)
    - For the blank assay double-click a position in the autoloader scheduler and select Category: **Calibration**; Type: **Blank**

- Monthly Tasks:
    - Refresh titrants.
        - Click **Refresh** in the Dispenser view.
        - Enter the volume and date.
        - Click **OK.**
        - Click **Yes** when screen display asks if help is required.
        - Remove the titrant bottle and refresh with new titrant.
    - KHP – Base Titrant Standardisation:
        - Accurately weigh 15 mg of KHP into a SiriusT3 assay vial.
        - Double-click a position in the autoloader scheduler to create a new assay.
        - Place a clean vial in the position.
        - Click the Category drop-down arrow and select **Calibration**.
        - Click the Type drop-down arrow and select **KHP**.
        - The base concentration factor is automatically refined and if the value is within the acceptable limits, it is automatically used for all subsequent assays. If the values are outside the acceptable limits, the assay is automatically rejected as an import default.

Setting up and designing assays using SiriusT3Control:

- Fast UV pK_a/psK_a assay:
    - Sample preparation:
        - Dispense 5 µL of a 10 mM sample solution (solvent: DMSO) into the sample vial.
    - Calibrate Fast UV buffer:
        - Choose a position on the autoloader deck and double click the corresponding position on the scheduler.
        - Select **Calibration** and **Fast UV Buffer Calibration** from the drop-down menu.
        - If a psK_a assay is performed select **Fast UV Buffer Calibration MeOH** from the Type drop-down menus.
        - Place the calibration vial in the position on the Autoloader tray that represents the position selected on the scheduler.
    - Design Sample Assay:

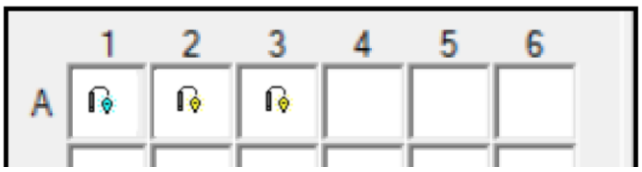

        - Choose a position on the autoloader deck and double click the corresponding position on the scheduler.
        - Select **pK_a** and **Fast UV pK_a** from the drop-down menus.
        - If a psK_a assay is performed select **Fast UV psK_a** from the Type drop-down menu.
        - Enter the sample model by clicking  (New Sample Wizard) and enter the sample details into the dialog box according to the directions in the following images:

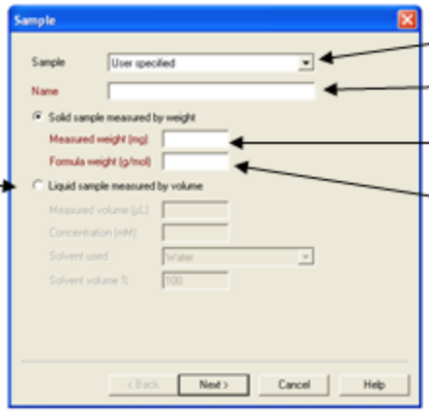

Select User specified

Enter Sample name

Enter weight of the sample

Enter full formula weight (including counterions, hydrates etc.)

If the sample is a liquid, select this radio button and enter the relevant details below

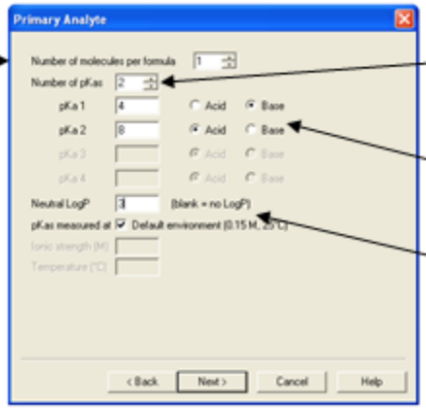

Enter number of molecules per formula. This is the stoichiometry of the sample molecule in the formula

Enter number of pK_as

Enter estimated value of pK_as and if they are acidic or basic.

Optionally, enter an estimated logP for the neutral form of the analyte

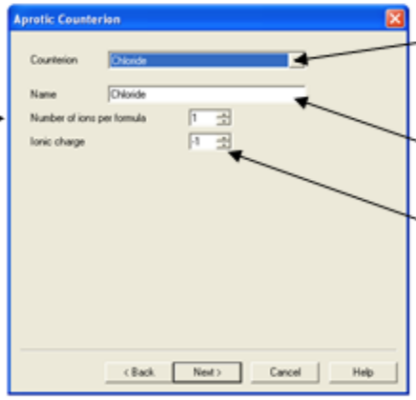

Either choose the Aprotic counterion from the drop-down list, or select "User specified" and manually enter a name.

Manually enter the aprotic counterion name

Enter the charge of the aprotic counterion

Enter number of ions per formula. This is the stoichiometry of the selected ion in the formula

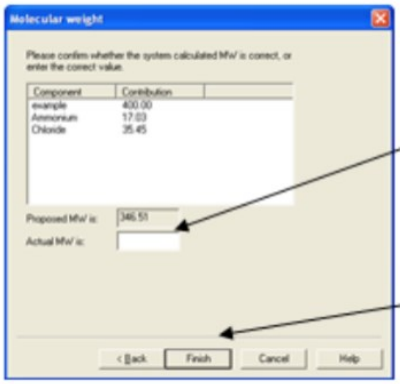

Check that the proposed molecular weight is correct.

Click Finish

- Set the titration direction ensuring that the assay begins at a pH where the sample is most soluble. (Bases: low to high; Acids: high to low; Ampholytes: whichever starting pH is furthest from a pK_a, e.g. set titration from high to low for a compound with pK_a at 3 and 8)
- Place sample vial in the position on the Autoloader tray that represents the position selected on the scheduler.
- Run the Fast UV pK_a/psK_a assay by selecting **Schedule tray to Run**, followed by **Start Running Assay** in the instrument menu.

- <u>UV-metric pK_a/psK_a assay:</u>
  - Sample preparation:
    - Dispense 5 µL of a 10 mM sample solution (solvent: DMSO) into the sample vial.
    - Pipette 5 µL DMSO into the blank vial.
    - Add 25 µL of phosphate buffer to both vials.
  - Design Sample Assay:

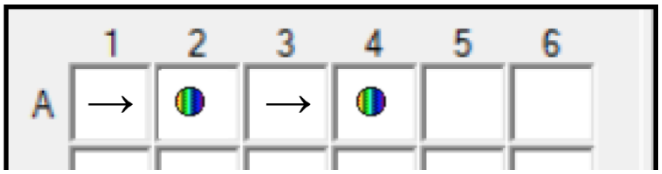

    - Choose a position on the autoloader deck and double click the corresponding position on the scheduler.
    - Select **pK_a** and **UV-metric pK_a** from the drop-down menus.
    - If a psK_a assay is performed select **UV-metric psK_a** from the Type drop-down menu.
    - Enter the sample model by clicking  (New Sample Wizard) and enter the sample details into the dialog box.
    - Set the titration direction (low to high for bases, high to low for acids).
    - Place two vials in adjacent positions on the Autoloader tray that represents the position selected on the scheduler. A blank measurement is performed prior to every sample measurement.
    - Run the UV-metric pK_a/psK_a assay by selecting **Schedule tray to Run**, followed by **Start Running Assay** in the instrument menu.

- <u>pH-metric pK_a/psK_a assay:</u>
  - Sample preparation:
    - Weigh in 0.5 to 1.0 mg of sample into a clean vial and take note of the exact weight.
  - Design Sample Assay:

    - Choose a position on the autoloader deck and double click the corresponding position on the scheduler.
    - Select **pK_a** and **pH-metric pK_a** from the drop-down menus.
    - If a psKa assay is performed select **pH-metric psK_a** from the Type drop-down menu.
    - Enter the sample model by clicking  (New Sample Wizard) and enter the sample details into the dialog box. Make sure to correctly add the exact weight, molecular weight and predicted pK_a values of the sample.
    - Set the titration direction (low to high for bases, high to low for acids).
    - After each pH-metric pK_a assay create a **Clean Up** assay.
    - Place sample vial in the position on the Autoloader tray that represents the position selected on the scheduler, followed by an empty clean-up vial.
    - Check if the sample has an appropriate concentration (check the buffer capacity plot in the What If section). The buffering of the sample (coloured lines) must exceed the buffering of water (black line) over a small pH interval.

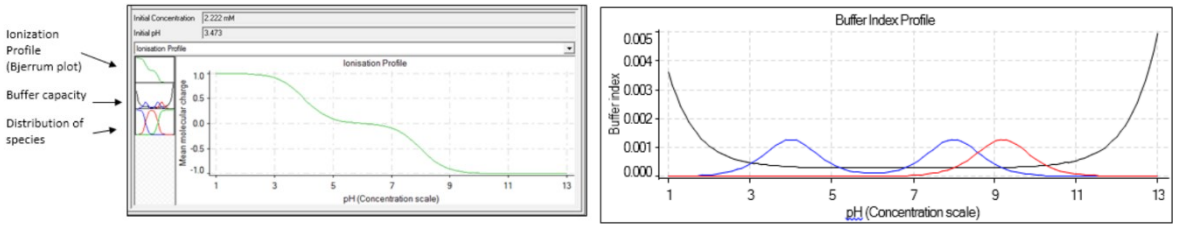

- If the buffering of the sample is below the buffer capacity line, the sample concentration must be increased.
- Run the pH-metric pK_a/psK_a assay by selecting **Schedule tray to Run**, followed by **Start Running Assay** in the instrument menu.

Data Refinement using SiriusT3Refine

- <u>pH-metric pK_a/psK_a refinement:</u>
  - Open pH-metric pK_a/psK_a dataset in the SiriusT3Refine software. A multi-titration pH-metric tab displays:

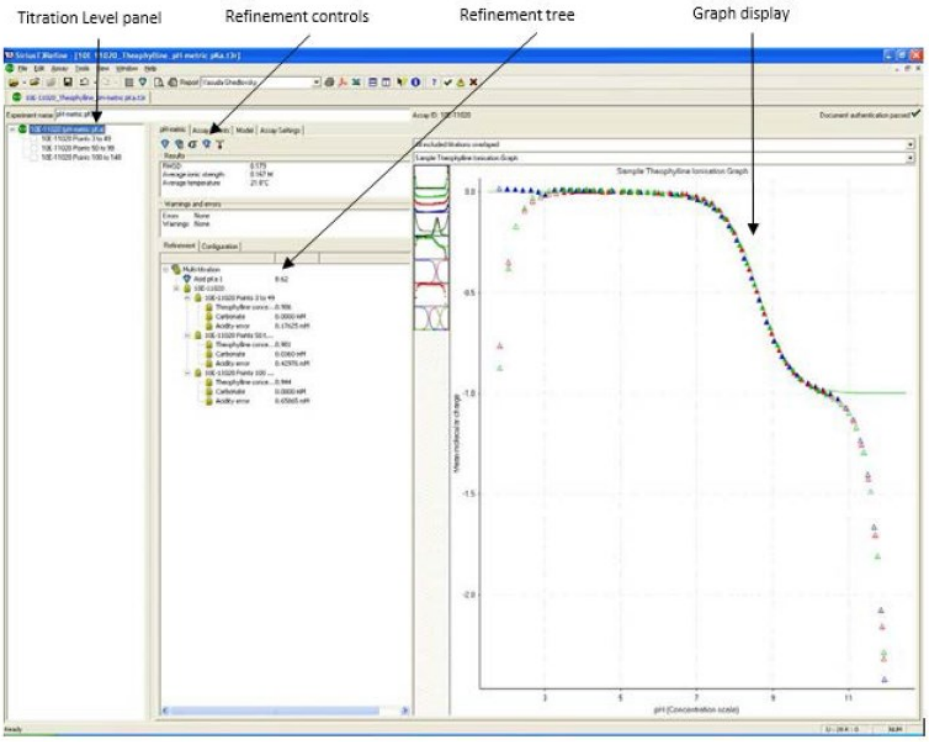

  - Single titration refinement:
    - Select the first of the three single titrations in the titration level panel.
    - Parameters with a ‘diamond’ symbol are allowed to vary during refinement.

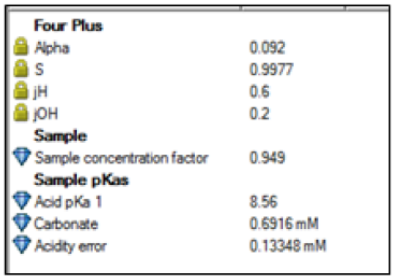

    - Right click the sample concentration factor in the refinement panel and select **Restore Default**.

- Repeat for sample pK_a(s), carbonate and acidity error parameters.
- Clip out noise data at extreme pHs.
- Hold Ctrl, left click and drag the cursor on the graph to generate a second set of clipping bars.
- Use the second set of clipping bars to clip out data that is (a) part of an ionisation curve and (b) in-line with the theoretical ionisation curve.

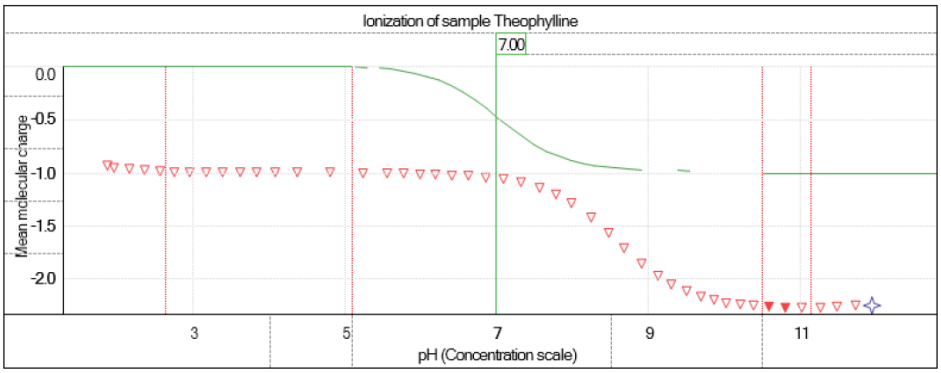

- Lock all parameters except the sample concentration factor and acidity error and click **Refine**. 
- If only one plateau is found, refine on the acidity error only.
- Remove the second set of clipping bars by dragging one bar on top of the other.
- Using the remaining clipping bars, clip out noisy data at extreme pHs, but ensure that data at pH 6 and 10 is included.

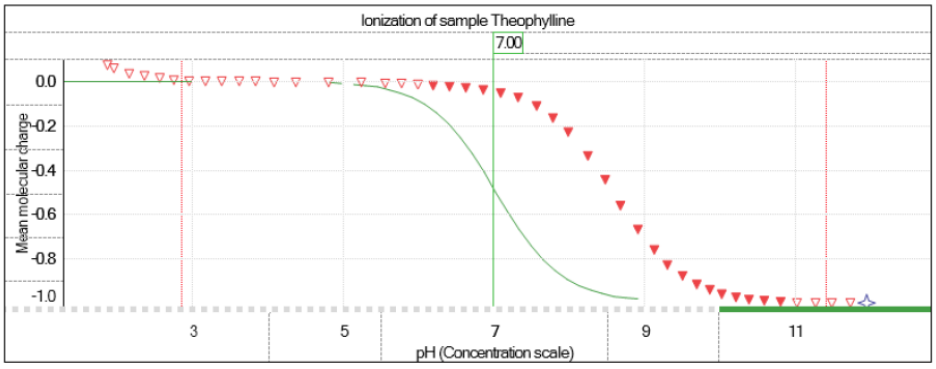

- Lock all parameters except for sample pK_a and carbonate concentration and click **Refine.**

- Unlock all parameters and click **Refine.**

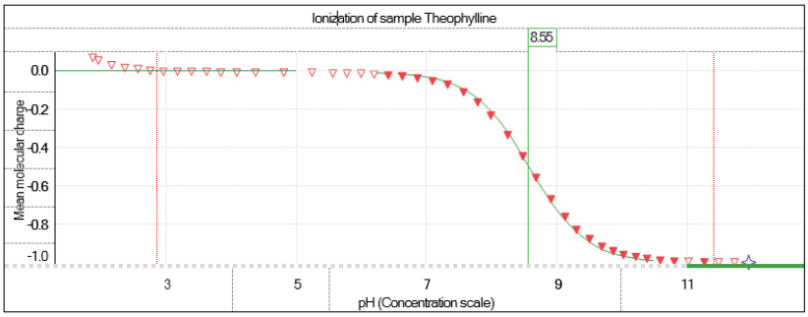

- If the curve is not ideally fitted to the theoretical ionisation profile restore the sample pK_a and carbonate concentration parameters to default, adjust the clipping bars to exclude noisy data and click Refine.
- Repeat these steps for the remaining two single-titrations.

  - Multi Titration Refinement:
    - After all individual titrations have been processed the final results may be calculated in the multi-titration pH-metric tab.
    - Click **Auto Refinement** 
    - Click  to determine the standard error for the result.
    - if a psK_a measurement with cosolvent was performed, the data from each titration is automatically plotted against the cosolvent ratio and a multi-titration refinement is not necessary.
  - If R^2 value is below 0.9 consider repeating the assay.

- <u>Fast UV and UV-metric pK_a/psK_a refinement:</u>
  - Open UV-metric pK_a file to display the UV pK_a tab.

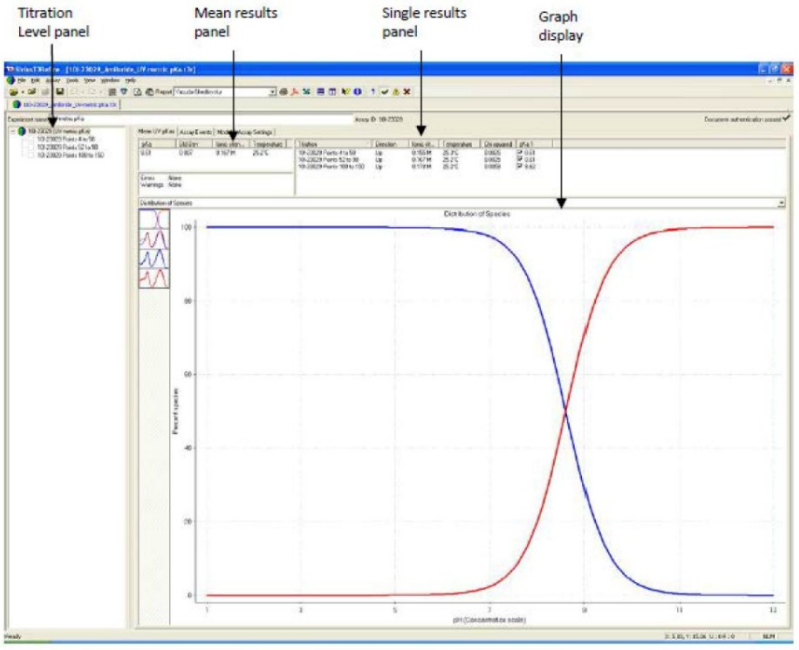

- Single Titration Refinement:
  - From the pH vs. absorbance graph exclude any noisy data at extreme pH.

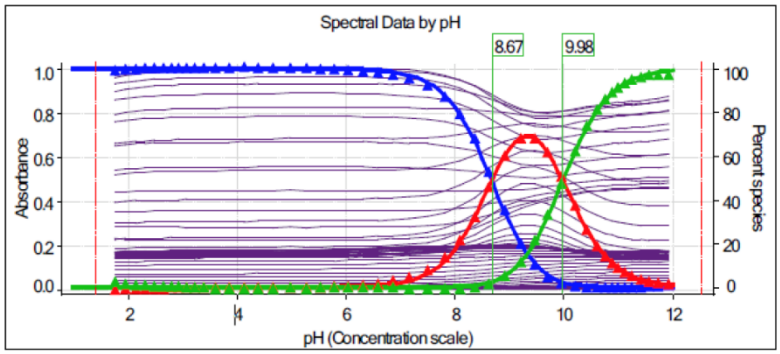

  - Exclude non-absorbed wavelengths from the wavelength vs. Absorbance graph.

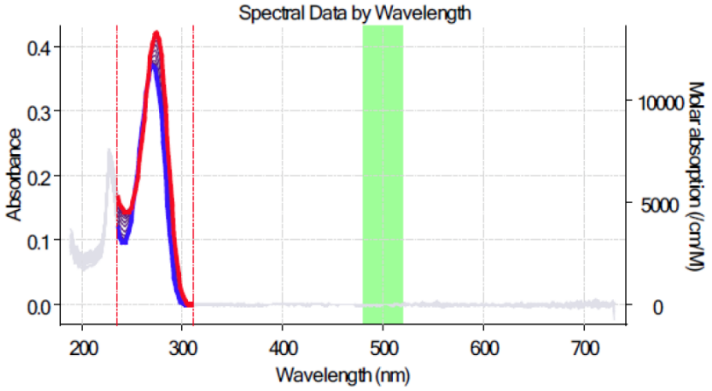

  - Process all individual titrations. The averaged result displays automatically on the Mean UV pK_as tab.

Instrument Shut Down to store SiriusT3 when not in use:

- Fill all reagent bottles with purified water.
- Perform a flush of the Dispenser Module with the purified water.
  - Set the volumes to 10 mL for 2.5 mL plungers and 3 mL for 0.5 mL plungers.
- Empty all reagent bottles.
- Perform a flush of the Dispenser Module with just air to clear the capillaries.
  - Set the volumes to 10 mL for 2.5 mL plungers and 3 mL for 0.5 mL plungers.
- Remove the electrode and place in a storage solution.
- Turn off the argon supply.
- Turn off and unplug the instrument.

- When restarting the system after prolonged storage, ensure fresh reagents are prepared prior to use.

7. REFERENCES

Pion Inc. SiriusT3 instruction manual (Rev. August 2019).
Pion Inc. Extended Instrument Shut Down for Pion SiriusT3 Storage Guidelines (2023). Retrieved from: SiriusT3 | Pion (pion-inc.com)

8. REVISION

Date	Version	Description of revision
24.02.2023	01	Creation and release

Bibliography

1. Mohs RC, Greig NH. Drug discovery and development: Role of basic biological research. Vol. 3, Alzheimer's and Dementia: Translational Research and Clinical Interventions. Elsevier Inc; 2017. p. 651–7.
2. Hughes JP, Rees SS, Kalindjian SB, Philpott KL. Principles of early drug discovery. Vol. 162, British Journal of Pharmacology. 2011. p. 1239–49.
3. Berdigaliyev N, Aljofan M. An overview of drug discovery and development. Vol. 12, Future Medicinal Chemistry. Future Medicine Ltd.; 2020. p. 939–47.
4. Pandey A. Overview Of All Phases In Drug Development And Discovery Process [Internet]. 2023 [cited 2023 Mar 8]. Available from: https://www.nebiolab.com/drug-discovery-and-development-process/
5. Talevi A, Quiroga PAM. ADME Processes in Pharmaceutical Sciences. Springer Nature Switzerland; 2018.
6. Talevi A. Computer-aided drug design: An overview. In: Methods in Molecular Biology. Humana Press Inc.; 2018. p. 1–19.
7. Abbott NJ, Patabendige AAK, Dolman DEM, Yusof SR, Begley DJ. Structure and function of the blood-brain barrier. Vol. 37, Neurobiology of Disease. 2010. p. 13–25.
8. Pandit R, Chen L, Götz J. The blood-brain barrier: Physiology and strategies for drug delivery. Vols. 165–166, Advanced Drug Delivery Reviews. Elsevier B.V.; 2020. p. 1–14.
9. Daneman R, Prat A. The blood–brain barrier. Cold Spring Harb Perspect Biol. 2015 Jan 1;7(1).
10. Vallianatou T, Giaginis C, Tsantili-Kakoulidou A. The impact of physicochemical and molecular properties in drug design: Navigation in the "Drug-Like" chemical space. Adv Exp Med Biol. 2015;822:187–94.
11. Hansch C, Fujita Vol T, Roberts RB, Cowie DB, Britten R, Abelson PH, et al. Analysis. A Method for the Correlation of Biological Activity and Chemical Structure [Internet]. Vol. 39, J. Biol. Chem. 1953. Available from: https://pubs.acs.org/sharingguidelines
12. Hansch C. A Quantitative Approach to Biochemical Structure-Activity Relationships. Acc Chem Res. 1969;2(8):232–9.
13. Yu LX, Amidon GL, Polli JE, Zhao H, Mehta MU, Conner DP, et al. Biopharmaceutics classification system: The scientific basis for biowaiver extensions. Vol. 19, Pharmaceutical Research. 2002. p. 921–5.
14. Pathare B, Tambe V, Patil V. A REVIEW ON VARIOUS ANALYTICAL METHODS USED IN DETERMINATION OF DISSOCIATION CONSTANT. Int J Pharm Pharm Sci. 2014;6(8):26–34.
15. Albert ASEP. The Determination of Ionization Constants: A Laboratory Manual. 3rd ed. New York: Chapman and Hall; 1984.
16. Reijenga J, van Hoof A, van Loon A, Teunissen B. Development of methods for the determination of pKa values. Vol. 8, Analytical Chemistry Insights. 2013. p. 53–71.

17. Henderson LJ. Concerning the relationship between the strength of acids and their capacity to preserve neutrality. American Journal of Physiology-Legacy Content. 1908;21(2):173–9.

18. Poduri R. Drug Discovery and Development [Internet]. Poduri R, editor. Singapore: Springer Singapore; 2021. Available from: https://link.springer.com/10.1007/978-981-15-5534-3

19. Wager TT, Hou X, Verhoest PR, Villalobos A. Central Nervous System Multiparameter Optimization Desirability: Application in Drug Discovery. ACS Chem Neurosci. 2016 Jun 15;7(6):767–75.

20. Lipinski CA, Lombardo F, Dominy BW, Feeney PJ. Experimental and computational approaches to estimate solubility and permeability in drug discovery and development q settings. Adv Drug Deliv Rev. 2001;46:3–26.

21. Lipinski CA. Lead- and drug-like compounds: The rule-of-five revolution. Vol. 1, Drug Discovery Today: Technologies. 2004. p. 337–41.

22. Wager TT, Hou X, Verhoest PR, Villalobos A. Moving beyond rules: The development of a central nervous system multiparameter optimization (CNS MPO) approach to enable alignment of druglike properties. ACS Chem Neurosci. 2010 Jun 16;1(6):435–49.

23. Nakov N, Acevska J, Brezovska K, Dimitrovska A. Overview on chromatographic and potentiometric based approaches for pKa determination of sparingly soluble substances. Macedonian Pharmaceutical Bulletin. 2018;63(02):21–7.

24. Kahlert H. Potentiometry. In: Electroanalytical Methods: Guide to Experiments and Applications. Springer Berlin Heidelberg; 2010. p. 237–56.

25. Völgyi G, Ruiz R, Box K, Comer J, Bosch E, Takács-Novák K. Potentiometric and spectrophotometric pKa determination of water-insoluble compounds: Validation study in a new cosolvent system. Anal Chim Acta. 2007 Feb 5;583(2):418–28.

26. Morris R. Spectrophotometry. Current Protocols in Essential Laboratory Techniques. 2015 Nov 1;11(1):2.1.1-2.1.30.

27. Manchester J, Walkup G, Rivin O, You Z. Evaluation of p K a estimation methods on 211 druglike compounds. J Chem Inf Model. 2010 Apr 26;50(4):565–71.

28. Balogh GT, Gyarmati B, Nagy B, Molnár L, Keseru GM. Comparative evaluation of in silico pKa prediction tools on the gold standard dataset. QSAR Comb Sci. 2009;28(10):1148–55.

29. Lee AC, Crippen GM. Predicting pKa. J Chem Inf Model. 2009 Sep 28;49(9):2013–33.

30. Bhal SK. >20 Years of Reliable pKa Predictions From ACD/Labs Accuracy Improvements & Customer Collaborations.

31. pKa calculation [Internet]. [cited 2023 Mar 8]. Available from: https://docs.chemaxon.com/display/docs/pka-calculation.md

32. Szegezdi J, Csizmadia F. Prediction of dissociation constant using microconstants. 2004.

33. Szegezdi J, Csizmadia F. A method for calculating the pKa values of small and large molecules. 2007.

34. Hollmann S, Frohme M, Endrullat C, Kremer A, D'Elia D, Regierer B, et al. Ten simple rules on how to write a standard operating procedure. Vol. 16, PLoS Computational Biology. Public Library of Science; 2020.

35. Cagigal E, González L, Alonso RM, Jiménez RM. pK a determination of angiotensin II receptor antagonists (ARA II) by spectrofluorimetry. J Pharm Biomed Anal. 2001;26(2):477–86.

36. Yellepeddi VK, Radhakrishnan J, Radhakrishnan R. Penetration and pharmacokinetics of non-steroidal anti-inflammatory drugs in rat prostate tissue. Prostate. 2018 Feb 1;78(2):80–5.

37. Dyakonov T, Muir A, Nasri H, Toops D, Fatmi A. Isolation and characterization of cetirizine degradation product: Mechanism of cetirizine oxidation. Pharm Res. 2010 Jul;27(7):1318–24.

38. Cignitti M, Ramusino MC, Rufini L. MOLECULAR STRUCTURE UV spectroscopic study and conformational analysis of domperidone. Vol. 350, Journal of Molecular Structure. 1995.

39. Malapero RJ, Zaccagnino MP, Brovman EY, Kaye AD, Urman RD. Etomidate derivatives: Novel pharmaceutical agents in anesthesia. Vol. 33, Journal of Anaesthesiology Clinical Pharmacology. Medknow Publications; 2017. p. 429–31.

40. Beijnen 'v2 JH, Holthuis JJM, Kerkdijk HG, Van Der Houwen OAGJ, Paalman ' ACA, Bult A, et al. Degradation kinetics of etoposide in aqueous solution. Vol. 41, International Journal of Pharmaceutics. 1988.

41. Grbic S, Parojcic J, Malenovic A, Djuric Z, Maksimovic M. A contribution to the glimepiride dissociation constant determination. J Chem Eng Data. 2010 Mar 11;55(3):1368–71.

42. Kadam Y, Yerramilli U, Bahadur A, Bahadur P. Micelles from PEO-PPO-PEO block copolymers as nanocontainers for solubilization of a poorly water soluble drug hydrochlorothiazide. Colloids Surf B Biointerfaces. 2011 Mar 1;83(1):49–57.

43. Mehmandoust M, Erk N, Karaman C, Karaman O. An electrochemical molecularly imprinted sensor based on CuBi2O4/rGO@MoS2 nanocomposite and its utilization for highly selective and sensitive for linagliptin assay. Chemosphere. 2022 Mar 1;291.

44. Takano A, Suhara T, Sudo Y, Inoue M, Hashimoto K, Zhang MR, et al. Comparative evaluation of two serotonin transporter ligands in the human brain: [11C](+)McN5652 and [11C]cyanoimipramine. Eur J Nucl Med. 2002;29(10):1289–97.

45. Tsutsumi S, Iida M, Tada N, Kojima T, Ikeda Y, Moriwaki T, et al. Characterization and evaluation of miconazole salts and cocrystals for improved physicochemical properties. Int J Pharm. 2011 Dec 15;421(2):230–6.

46. Schönherr D, Wollatz U, Haznar-Garbacz D, Hanke U, Box KJ, Taylor R, et al. Characterisation of selected active agents regarding pKa values, solubility concentrations and pH profiles by SiriusT3. European Journal of Pharmaceutics and Biopharmaceutics. 2015;92:155–70.

47. Sorasuchart W, Wardrop J, Ayres JW. Current address: Analytical Development Center [Internet]. Vol. 25, Drug Development and Industrial Pharmacy. 1999. Available from: www.dekker.com

48. Liao X, Wiedmann TS. Solubilization of Cationic Drugs in Lung Surfactant. Pharm Res. 2003;20:1858–63.

49. Altriat KD, Simpson CF. Analysis of some pharmaceuticals by high voltage capillary zone electrophoresis". Vol. 6, Jotmud of Pharmaceutical & Biomedical Analysis. 1988.

50. Seeman P. Cannabidiol is a partial agonist at dopamine D2High receptors, predicting its antipsychotic clinical dose. Transl Psychiatry. 2016;6(10).

51. Settimo L, Bellman K, Knegtel RMA. Comparison of the accuracy of experimental and predicted pKa values of basic and acidic compounds. Pharm Res. 2014;31(4):1082–95.

52. Bao X, Lu S, Liow JS, Morse CL, Anderson KB, Zoghbi SS, et al. [11C]Rhodamine-123: Synthesis and biodistribution in rodents. Nucl Med Biol. 2012 Nov;39(8):1128–36.

53. Taylor PJ, Cruickshank JM. Distribution coefficients of atenolol and sotalol. Vol. 37, Journal of Pharmacy and Pharmacology. 1985. p. 143–4.

54. Derendorf,' H, Rohdewald,' P, Hochhaus G, Mallmann H. HPLC determination of glucocorticoid alcohols, their phosphates and hydrocortisone in aqueous solutions and biological fluids. Vol. 4, Journal of Pharmaceutical & Biomedical Analysis. 1986.

55. Settimo L, Bellman K, Knegtel RMA. Comparison of the accuracy of experimental and predicted pKa values of basic and acidic compounds. Pharm Res. 2014;31(4):1082–95.

56. Luurtsema G, Schuit RC, Takkenkamp K, Lubberink M, Hendrikse NH, Windhorst AD, et al. Peripheral metabolism of [18F]FDDNP and cerebral uptake of its labelled metabolites. Nucl Med Biol. 2008 Nov;35(8):869–74.

57. Chauveau F, Boutin H, Van Camp N, Dollé F, Tavitian B. Nuclear imaging of neuroinflammation: A comprehensive review of [11C]PK11195 challengers. Vol. 35, European Journal of Nuclear Medicine and Molecular Imaging. 2008. p. 2304–19.

58. Voss LJ, van Kan C, Sleigh JW. Quantification of Neocortical Slice Diffusion Characteristics Using Pharmacokinetic and Pharmacodynamic Modelling. ISRN Neurosci. 2013 Sep 5;2013:1–5.

59. Bourdier T, Pham TQ, Henderson D, Jackson T, Lam P, Izard M, et al. Automated radiosynthesis of [18F]PBR111 and [18F]PBR102 using the Tracerlab FXFN and Tracerlab MXFDG module for imaging the peripheral benzodiazepine receptor with PET. Applied Radiation and Isotopes. 2012 Jan;70(1):176–83.

60. Huang WS, Huang SY, Ho PS, Ma KH, Huang YY, Yeh C Bin, et al. PET imaging of the brain serotonin transporters (SERT) with N,N-dimethyl-2-(2-amino-4-[18F]fluorophenylthio)benzylamine (4-[18F]-ADAM) in humans: A preliminary study. Eur J Nucl Med Mol Imaging. 2013 Jan;40(1):115–24.

61. Laruelle M, Abi-Dargham A, Van Dyck C, Gil R, Cyril D'souza D, Krystal J, et al. Dopamine and Serotonin Transporters in Patients with Schizophrenia: An Imaging Study with [123 I]-CIT. Vol. 47, Biol Psychiatry. 2000.

62. Ettlinger DE, Häusler D, Wadsak W, Girschele F, Sindelar KM, Mien LK, et al. Metabolism and autoradiographic evaluation of [18F]FE@CIT: a Comparison with [123I]β-CIT and [123I]FP-CIT. Nucl Med Biol. 2008 May;35(4):475–9.

63. Ziebell M, Thomsen G, Knudsen GM, De Nijs R, Svarer C, Wagner A, et al. Reproducibility of [123I]PE2I binding to dopamine transporters with SPECT. Eur J Nucl Med Mol Imaging. 2007 Jan;34(1):101–9.

64. Breuil L, Goutal S, Marie S, Del Vecchio A, Audisio D, Soyer A, et al. Comparison of the Blood–Brain Barrier Transport and Vulnerability to P-Glycoprotein-Mediated Drug–Drug Interaction of Domperidone versus Metoclopramide Assessed Using In Vitro Assay and PET Imaging. Pharmaceutics. 2022 Aug 1;14(8).

65. Laurens C, Abot A, Delarue A, Knauf C. Central effects of beta-blockers may be due to nitric oxide and hydrogen peroxide release independently of their ability to cross the blood-brain barrier. Front Neurosci. 2019;13(JAN).

66. Arendt RM, Greenblatt DJ, deJong RH, Bonin JD, Abernethy DR. Pharmacokinetics, central nervous system uptake, and lipid solubility of propranolol, acebutolol, and sotalol. Cardiology. 1984;71(6):307–14.